



ON THE DESIGN OF CAVITATION SUSCEPTIBILITY METERS (C.S.M.'s)

by Luca d'Agostino and A. J. Acosta
California Institute of Technology

for presentation at
the 20th American Towing Tank Conference
1983

Abstract

The observation of cavitation in C.S.M.'s at the throat of a Venturi tube provides an ideally simple and direct method to monitor the liquid quality in terms of the concentration of unstable nuclei as a function of the applied tension. In the previous work, of Oldenzien and Lecoffre, the use of C.S.M.'s was limited to the measurement of the tensile strength of the weakest nuclei present in the liquid. The purpose of the current ^(THIS) research ~~is to~~ extend this application to determine the concentration of unstable cavitation nuclei as a function of the applied tension over a wide range so that the nuclei number distribution can be derived. Various approximations are made to construct a simplified but still representative physical model of C.S.M.'s. ^{these} factors included the liquid sample initial conditions and properties, critical tension and concentration of cavitation nuclei (i.e. liquid quality) and required accuracy and range of the nuclei concentration measurement. The overall performance of C.S.M.'s is described in terms of a set of dependent parameters including the volume flux, velocity and pressure at the throat and at the exit (these are fluid mechanical parameters); the throat volume, diameter and length, and exit diameter (geometrical parameters); cavitation rate and bubble response time (cavitation parameters); error due to the interference of more than one nucleus simultaneously present in the cavitation region and error due

(over)

to the finite time duration of the observation (statistical parameters); nuclei concentration measurement, sample volume and sampling time (measuring process parameters in general). The relative dependence of these parameters is investigated. A simple quasi one-dimensional model is used to analyze the flow. Viscous effects in the venturi tube are estimated by matching an axisymmetric boundary layer with an ideal flow solution in order to demonstrate the presence of a potential core in the throat section where cavitation is to occur. The dynamics of a spherical bubble growing and travelling in a semi-infinite pipe are used to deduce both the critical tension and the response time of cavitation nuclei. The occurrence of nuclei in the cavitation region and the observation of cavitation events are treated as stochastic processes of Poisson's type in space and time, respectively. On the basis of the assumed nuclei number distribution, the expected errors due to nuclei interference and to finite observation time are thus related to the volume of the cavitation region and to the duration of the observation itself.

Finally, it is shown that these parameters can be organized into a functional network, leading to a systematic representation of the C.S.M. design problem.

The most important deductions are that:

- (1) the pressure in the cavitation region is an extremely sensitive parameter and cannot be directly measured with the necessary accuracy. It is therefore proposed to deduce the pressure from the potential core velocity at the throat obtained by using a L.D.V.;
- (2) the volume of the cavitation region must be reduced as much as possible in order to increase the applied tension without incurring in

- large errors due to nuclei interference;

(3) the time response of cavitation nuclei imposes a lower bound for the length of the cavitation region.

Preliminary tests of a prototype venturi made of acrylic plastic showed that the flow in the inlet can sustain, without separation, the very steep and large contraction suggested by design considerations, but that it is extremely sensitive to separation in the diffuser section following the test volume.

INTRODUCTION

Early studies have shown [5] that the maximum tensile strength that liquids can sustain is considerably reduced by the presence of weak spots, generically called "nuclei". Although their nature has not yet been fully understood, it has been recognized that small gas bubbles, certain types of solid impurities, and gas pockets contained inside crevices and cracks of a liquid-solid interface are nuclei, since they act as preferred points for the onset of liquid rupture.

The presence of nuclei is considerably important in many flows of technical interest, where they are responsible for originating or variously modifying the occurrence of cavitation, a generally undesired phenomenon which severely limits the performances of hydraulic operating machinery. In this respect the number of nuclei which become unstable at a given level of tension is therefore a fundamental parameter in the attempt both to predict the onset of cavitation and to deduce scaling laws capable of extending the results obtained from model tests to full-scale operation.

The effect of the presence of nuclei in liquids is not limited to cavitation. Inhomogeneities and, in particular, micro-bubbles, considerably change the optical and acoustical properties of liquids in a way which also depends in general on their concentration and size distribution [6]. Such phenomena, as well as cavitation, are of great practical importance in many technological applications of underwater acoustics and optics.

Therefore significant efforts have been made in developing methods to detect nuclei contained within liquids, whose effects usually dominate the ones due to the nuclei localized at the flow boundaries.

Some methods, such as photography or holography, which produce a recorded image of a sample volume in the liquid, allow one to detect nuclei whose size is larger than about 10 μm . They also can discriminate between bubbles and particles, but have the disadvantage that results are not immediately and continuously available because the analysis of the obtained data requires a considerable time.

Other methods, based upon optical or acoustical radiation scattered by the nuclei, can operate continuously providing results which are readily available, but do not allow one to distinguish readily between bubbles and particles. For satisfactory operation, a careful calibration using a liquid sample of known characteristics is needed. Non uniform illumination and finite size of the scattering volume may also generate systematic errors which are difficult to take into account. Besides, when particles are prevalent, considerable uncertainty is introduced by the fact that both their shape and index of refraction are unknown.

Bubbles in liquids can also be detected from the large attenuation experienced by acoustical radiation which resonates with the bubble natural frequency of volume oscillation. Detection systems based on this concept do not require long times for data analysis, but are unable to detect particles and need comparatively large and homogeneous sample volumes.

For the purpose of cavitation research, a common disadvantage of all the above methods is that only size distribution and concentration of the nuclei are measured. The value of the critical tension that makes each nucleus unstable, as required for cavitation studies, must therefore be deduced indirectly from size measurements, which can be done only in the case of micro-bubbles. Solid particles, when detected and recognized, can be included or not in the measurement of nuclei concentration, but no information is provided about their critical tension, yet it is known that only part of the solid particulates are active as cavitation nuclei.

To overcome these difficulties, cavitation events occurring in a known pressure field can be detected and counted. When applied to bodies of standardized form and size, this method has indeed the advantage of providing a direct measurement. However, since many nuclei are simultaneously exposed to the tension, the response of the weakest ones inevitably dominates the flow, so that only cavitation susceptibility evaluations can be obtained.

Recently Oldenziel, [1], [2], [3], [4], proposed a new instrument, the Cavitation Susceptibility Meter (C.S.M.), in which the internal flow of a liquid through a glass venturi is used to induce cavitation at the throat and bubbles are detected optically. The C.S.M. developed by Lecoffre at Neyrtec, [13], is based on the same principle, but it utilizes a stainless steel

venturi, where cavitation bubbles are counted by recording the noise generated by their collapse in the diffuser downstream the throat section.

Various methods to monitor the cavitation nuclei population of water samples, including the above two C.S.M.'s, have been recently compared together at Delft Hydraulics Laboratory [4]. The results confirm that C.S.M.'s can reliably measure the critical tension of the weakest nuclei and their concentration up to a maximum of the order of 10 cm^{-3} , after which the venturi throat becomes saturated with bubbles and the flow chokes. Reportedly the Neyrtec system can also measure the nuclei critical pressure in the range 0 bar to -2 bar without incurring in saturation, provided that the concentration of unstable nuclei does not exceed about 1 cm^{-3} . Nevertheless such low values of the pressure correspond to bubbles having an equilibrium radius between .1 and $1 \mu\text{m}$, whose concentration in most water samples is expected to be considerably larger than 1 cm^{-3} . Therefore it appears that, during operation in these conditions, several unstable nuclei are simultaneously present in the cavitation region of the C.S.M. When this happens, the pressure in the throat increases significantly with respect to its nominal steady state non-cavitating value. The C.S.M. is then partially saturated and the actual range over which reliable measurements of both the nuclei critical tension and concentration are possible is significantly reduced.

Yet, when compared to other techniques, C.S.M.'s seem to have several attractive features:

- (i) they provide a direct measure of both the nuclei critical tension and concentration, thus eliminating the problem of the uncertain behaviour of particles as cavitation nuclei;

- (ii) data analysis only requires a comparatively short time, so that the measure can be carried out in an almost continuous way;
- (iii) there is no limitation on the size of the smallest detectable nuclei.

On the other hand, successful operation of C.S.M.'s is severely limited by the nuclei concentration compared to the other techniques mentioned. But, because the C.S.M. is such a promising device in cavitation research, we have concerned ourselves in the present paper with all of the various considerations necessary for a reliable measurement to be made. We present these thoughts here in the hope that they will be useful since there is little discussion of these considerations in the literature.

C.S.M. OPERATION ANALYSIS

General Approach

The configuration of the axisymmetric C.S.M. venturi pipe considered in the present study is shown in Fig. 1. The flow originates from the far field on the left (subscript o), representing the sampled liquid, to the exhaust region on the right (subscript ex). Both the upstream and downstream conditions are supposed to be time-independent. A volume flux $Q(t)$ of liquid flows with axial velocity $u(x,r,t)$ and radial velocity $v(x,r,t)$ through the duct of local radius $B(x)$ and cross-sectional area $A(x) = \pi B^2(x)$, divided in five segments: a cylindrical inlet (subscript i), a contraction (subscript c), a cylindrical throat (subscript t), a diffuser inlet (subscript di) and a conical diffuser (subscript de). The length L of each segment of the duct is shown in the same figure; contraction area ratio is: $C_r = A_t / A_i$ and the

diffuser area ratio (expansion ratio) is: $C_e = A_{ex} / A_t$.

The main parameters used to describe the overall performance of C.S.M.'s are shown in the block diagram of Fig. 2. The existence of functional relations between two parameters is indicated by arrows connecting the two corresponding blocks. The nature of these relations will be discussed in detail later.

Some of the parameters in the diagram represent given data, some can be considered as independent requirements and some as resulting or dependent factors. However, the subdivision in such categories is somewhat arbitrary, since it depends on the view point chosen to approach the whole problem of C.S.M. design. The one implicitly adopted in most of the present analysis can be summarized as follows:

- first it is assumed that the sample initial conditions and properties are given;

- second a nuclei number distribution (i.e. the liquid quality) of the sample is postulated, which is generally representative of typical water samples of technological interest;

- finally a set of conditions on the remaining dependent parameters is deduced for the measurement of unstable nuclei concentration to be possible over the assigned or assumed nuclei radius range with the required precision.

This point of view is particularly useful for design orientation. On the other hand, for performance assessment of a given design, the obtainable precision in the measurement of unstable nuclei concentration over a certain radius range is the result of the specific C.S.M. geometry which can be

analyzed with the methods contained herein.

Liquid Quality and Critical Tension

In cavitation research literature the liquid quality of a sample is usually expressed by means of the nuclei number distribution: $N(R_o) = -dn/dR_o$, where $n(R_o)$ is the number concentration of nuclei whose equilibrium radius is not smaller than R_o . The nuclei number distributions of water samples of technological interest spread in practice over a very large range. Here, for simplicity, we assume: $N(R_o) = K_{dis} / R_o^3$, where $K_{dis} = 10^{-4}$ to 10^{-3} m^{-1} (typically $K_{dis} = 10^{-3} \text{ m}^{-1}$), which is in the average representative of the data reported in the literature in the radius range 10 to 100 μm . Thus it follows that

$$n(R_o) = \frac{K_{dis}}{2R_o^2} \quad (1)$$

In order to relate the nuclei number distribution to the corresponding critical pressure, we make the hypothesis that all the nuclei consist of equilibrium gas bubbles, for which the critical tension with respect to dynamic stability, [5], is expressed by:

$$(p_v - p)_{cr} = 4 \frac{S}{3 R_o} \left[3 \left(1 + \frac{p_o - p_v}{2 S / R_o} \right) \right]^{-1/2} \quad (2)$$

where p_o and R_o are the equilibrium pressure and radius of the bubble, p_v is the vapor pressure and S the surface tension (see Fig. 3). The corresponding "critical" velocity at the venturi throat deduced from ideal, incompressible, steady flow calculations is shown in Fig. 4. Similarly, the exhaust pressure coefficient $C_{pex} = (p_{ex} - p_v) / (p_o - p_v)$ is plotted in Fig. 5 for the case $p_o = 1$

bar and various expansion ratios. When the equilibrium pressure p_0 increases, the C_{pex} curves shift to the left in the diagram.

Note that the critical tensions of bubbles in the size range of interest (say 10 to 100 μm) are quite small. Also note, on the other hand, that, on the same range, the radius of marginally stable bubbles (critical radius) is a very sensitive function of the applied tension. These facts have several important (and unfortunate) consequences for the design of C.S.M.'s. The first is that it is virtually impossible to measure these small pressures at the throat because of inadequate sensitivity and, if done intrusively, separation or cavitation may be induced. The second is that the throat pressure must be evaluated accurately to avoid large errors in the determination of the nuclei number distribution. A third consequence has to do with the problem of regulating the flow by varying the exhaust pressure. The curves of Fig. 5 deduced for $p_0 = 1$ bar show that very low sensitivity is obtained, unless diffusers with a very small expansion ratio are used. Besides, due to the shift of the curves to the left when the equilibrium pressure p_0 increases, the same sensitivity cannot be achieved throughout the radius range of interest with the same diffuser geometry which can be analyzed with the methods contained herein.

Saturation and Throat Section Volume

As pointed out briefly in the introduction, the problem of saturation poses a significant limitation to the operation of C.S.M.'s. It also introduces a systematic error, since the unsteady pressure perturbations do to the presence of a growing or collapsing bubble in the cavitation region of the C.S.M. can prevent the normal growth of other neighbouring nuclei.

To control such an error the probability of finding more than one unstable nucleus in the low pressure volume, V_{1p} , of the C.S.M. must be minimized. When the nuclei concentration is uniform, the occurrence of m unstable nuclei in V_{1p} is expected to follow the Poisson distribution:

$$\text{Pr}(m) = \frac{N_{ub}^m}{m!} e^{-N_{ub}} \quad (3)$$

where $N_{ub} = n(R_0) V_{1p}$ is the average number of unstable nuclei in V_{1p} . Therefore the cumulative probability of observing two or more unstable nuclei in V_{1p} (bubble interference probability, see Fig. 6) is:

$$\beta = 1 - \text{Pr}(0) - \text{Pr}(1) = 1 - (1 + N_{ub}) e^{-N_{ub}} \quad (4)$$

It is now possible to express the low pressure volume of the C.S.M. as a function of the equilibrium bubble radius and of the bubble interference probability. The results of Fig. 7 show that, in the radius range 10 to 100 μm , if the error is to be reduced to an acceptable level, the volume of the cavitation region of the C.S.M. should not exceed about 50 mm^3 .

Bubble Dynamic Response and Throat Section Geometry

The problem of the response of an isolated bubble in the throat of the C.S.M. is now addressed. The solution of such a problem in terms of the detection time, T_{det} , and detection length, L_{det} (respectively defined as the time and the length necessary for the bubble to grow to a detectable radius size, R_{det}), will be used to estimate the minimum length of the low pressure volume, thus completing the geometrical definition of this component.

A number of assumptions are made in order to construct a simplified set of equations which nevertheless models the interactions between the bubble and the liquid. First the flow is supposed to be one-dimensional, ideal, incompressible and the relative motion of the bubble with respect to the liquid is neglected. The bubble, moving along the centerline of the duct with instantaneous position $x_b(t)$, remains spherical and its radius $R(t)$ is determined by the Rayleigh-Plesset equation [7]:

$$p_v - p_b = \rho \left[R \frac{d^2 R}{dt^2} + \frac{3}{2} \left(\frac{dR}{dt} \right)^2 \right] - p_g \left(\frac{R_0}{R} \right)^3 + 2 \frac{S}{R} \quad (5)$$

where S is the surface tension and diffusive and thermal effects are neglected (p_v and p_g are constant). Here p_b is the external pressure driving the bubble volume changes and it is assumed to be about equal to the pressure of the liquid in the proximity of the bubble. Then, from the continuity and unsteady Bernoulli's equations for the flow upstream (subscript u) and downstream (subscript d) the bubble:

$$Q_u - Q_b + 2 \pi R^2 \frac{dR}{dt} = 0 \quad (6)$$

$$Q_d - Q_b - 2 \pi R^2 \frac{dR}{dt} = 0 \quad (7)$$

$$- I_u \frac{dQ_u}{dt} + \frac{p_0 - p_b}{\rho} - \frac{1}{2} \frac{Q_b^2}{A_b^2} = 0 \quad (8)$$

$$- I_d \frac{dQ_d}{dt} + \frac{p_b - p_{ex}}{\rho} + \frac{1}{2} \frac{Q_b^2}{A_b^2} - \frac{Q_d^2}{A_d^2} = 0 \quad (9)$$

where $A_b = A(x_b)$, p_0 and p_{ex} are constant and:

$$I_u \simeq \int_{x_1}^{x_b} \frac{dx}{A(x)} ; \quad I_d \simeq \int_{x_b}^{x_6} \frac{dx}{A(x)} \quad (10)$$

Equations (6) through (9) are then transformed by introducing perturbation quantities with respect to the steady state solution and linearized for small changes in the volume fluxes. Finally, if $I_u \simeq x_b / A_b = u_t t / A_t \ll I_u + I_d$, which is essentially equivalent to consider the dynamics of a bubble entering a semi-infinite pipe of constant cross-sectional area A_t , the perturbation and Rayleigh-Plesset equations can be reduced to the following 2nd order differential equation for the bubble radius $R(t)$:

$$\frac{2 \pi \rho u_t}{A_t} \left[2 t R^2 \frac{d^2 R}{dt^2} + 4 t R \left(\frac{dR}{dt} \right)^2 + R^2 \frac{dR}{dt} \right] + \rho R \frac{d^2 R}{dt^2} + \frac{3}{2} \rho \left(\frac{dR}{dt} \right)^2 +$$

$$- p_v - p_g \left(\frac{R_0}{R} \right)^3 + 2 \frac{S}{R} + p_t = 0 \quad (11)$$

where p_t and u_t are the steady state pressure and velocity at the throat. The detection time, T_{det} , and detection length, L_{det} , computed for a detection radius $R_{det} = 150 \mu m$ and a throat diameter $D_t = 1 mm$ by numerically integrating the above equation, are shown in Fig. 8 and Fig. 9. The maximum in the results separates two regimes: in the lower radius range the inertial effects of the displaced liquid dominate, while in the upper one the effect of bubble gas content prevails, therefore accelerating the bubble dynamic response. Note that, in the radius range of interest, the detection length is almost independent of the equilibrium bubble pressure and that the length of the throat section should not be shorter than 5 to 10 mm. Also note that the solution of the above equation depends on A_t , the throat cross-sectional area. Therefore, if the low pressure volume is initially fixed in order to properly

limit the bubble interaction probability, some iteration on the throat diameter may be required to completely define the geometry of the C.S.M. low pressure volume.

Cavitation Rate and Unstable Nuclei Concentration Measurement

Once the throat cross-sectional area has been determined, the volume flux: $q = u_t A_t$ and the mean cavitation event rate $\dot{V}_c = Q n(R_0)$ can be computed. Results shown in Fig. 10 and Fig. 11 for a throat diameter $D_t = 1$ mm indicate that, in the radius range from 10 to 100 μm , as many as a few hundreds of cavitation events per second are to be expected.

For a given pressure at the throat, the corresponding concentration of unstable nuclei can be estimated from the count of the cavitation bubbles observed during the sampling time. In steady state conditions, if the liquid quality of the sample is constant, the occurrence of m cavitation events in the time interval T_s (sampling time) is expected to follow the Poisson distribution with parameter $\xi = \dot{V}_c T_s$, equal to the average number of events in the same time. Since T_s can be conveniently measured, the problem of estimating \dot{V}_c now reduces to the estimation of ξ .

It is known from the theory of probability distributions, [11], that the best estimator of the Poisson parameter is the observed frequency m , whose variance is: $V[m] = \xi$ and $(1 - \alpha)$ confidence limits are given by:

$$\xi_1 = \frac{1}{2} \chi^2_{\alpha/2}(2m) ; \quad \xi_2 = \frac{1}{2} \chi^2_{\alpha/2}(2m + 2) \quad (12)$$

where $\chi^2_p(q)$ is the p -percentile of the χ^2 distribution with q degrees of freedom (see Fig. 12). Thus, one way to assess the relative indetermination in the

estimate of ξ consists in normalizing the confidence interval with respect to the corresponding observed frequency (see Fig. 13, where $\alpha = .20$). Another less rigorous method uses the estimated root mean square (r.m.s.) error of the observed frequency $\sqrt{m} \simeq \sqrt{V[m]}$ instead of the confidence interval. The results of this second case are presented in Fig. 14 and comparison with Fig. 13 shows that the two methods are essentially equivalent for large observed frequencies ($m > 30$), apart from a scaling factor. Indeed the agreement could be made closer by simply adjusting the confidence level $1 - \alpha$. Because of its simplicity, the second method is used here. Then, if ε is the estimated r.m.s. relative error in the measurement of λ_c (or any other linearly related quantity, like $n(R_0)$ and $N(R_0)$), the necessary sampling time: $T_s = 1 / \lambda_c \varepsilon^2$ and liquid volume: $V_s = Q T_s$ are plotted in Fig. 15, 16 and 17. From them it appears that the liquid sample volume and sampling time required for one single measurement of unstable nuclei concentration of acceptable precision are at most of the order of 10 dm^3 and 10 sec respectively. Of course, the overall sampling time and volume of the liquid necessary for the evaluation of the nuclei number distribution will depend on the total choice of number of points where the measurement of the unstable nuclei concentration is carried out.

Viscous Effects and Separation

It was previously mentioned that one of the most difficult problems of C.S.M.'s consists in measuring the throat pressure with the required precision. Since direct measurements are virtually impossible, indirect methods must be used. Most naturally the throat pressure may be deduced from velocity measurements by using Bernoulli's equation. An unavoidable problem associated

with this technique is that the throat pressure, being inherently small compared to the total and kinetic pressures, is expressed as the difference of two almost equal quantities. Thus, relative errors in the evaluation of such quantities lead to a larger relative error for the throat pressure.

In existing C.S.M.'s, [1], [2], [3], [4], the velocity measurement was carried out in the inlet section of the duct, upstream of the contraction. This method appears to be rather unsatisfactory for various reasons. First, any intrinsic error in the measurement of the upstream velocity or due to inaccurate estimate of boundary layer effects is amplified proportionally to the contraction ratio when the throat velocity is derived from continuity arguments. This limitation is particularly severe since in C.S.M.'s the contraction ratio should be as large as possible in order not to appreciably affect the condition of the sampled liquid during its flow in the inlet section. Moreover, it is generally necessary to make the inlet section longer, which also is likely to affect the conditions of the sampled liquid, especially when a second venturi of smaller contraction ratio is used to monitor the velocity.

These difficulties are overcome if the velocity measurement is carried out at the throat. In consideration of the various requirements and limitations involved, the use of a laser Doppler velocimeter (L.D.V.) presently seems to be the best solution. But, for the pressure to be deduced from velocity measurements, the presence of a potential core at the C.S.M. throat must be demonstrated. Viscous effects have therefore been estimated by matching an axisymmetric boundary layer, [10], with the quasi one-dimensional ideal flow solution based on the duct geometry, [8], [9]. The duct radius $B(x)$ has been assumed to be continuous with continuous first and second derivatives, as

required by fluid mechanical considerations to avoid separation. In the contraction and diffuser inlet sections $B(x)$ was supposed to have sinusoidal second derivative. The inlet and throat sections were taken to be cylindrical and the diffuser exit section to be conical, of given semi-aperture angle. The length of each section has also been specified in terms of the inlet duct radius.

The results of such boundary layer calculations obtained for a prototype venturi made of acrylic plastic with Reynolds number based on the inlet radius and average velocity $Re_i = 700$ (the lowest expected value during operation) are summarized in Fig. 18 through 22. The geometrical characteristics of the above prototype venturi are: $L_i = 11.4$ mm, $L_c = 10.4$ mm, $L_t = 7.7$ mm, $L_{di} = 3$ mm, $L_{de} = 6.6$ mm, $\beta_d = .80$ deg, $D_t = 1$ mm, $C_r = 100$, $D_{ex} / D_t = 1.23$ and the duct shape profile is shown in Fig. 18, where the scales on the two axes are different. The boundary layer displacement and momentum thicknesses plotted in Fig. 19 (normalized with respect to the inlet radius) and in Fig. 20 (normalized with respect to the local duct radius) clearly demonstrate the presence of a potential core in the throat section of the C.S.M. In Fig. 21 the pressure coefficients at the centerline, C_{pcl} , and at the boundary layer edge, C_{ped} , are shown as functions of the axial coordinate of the duct. Here the pressure is normalized with respect to the inlet pressure and velocity. Note the very steep pressure drop in the contraction and the milder recovery in the diffuser.

Two kinds of problems may be expected in the venturi as a consequence of viscous effects. If the contraction is too steep, Taylor-Görtler instability may develop, and, if too large negative pressure gradients are present, flow separation may occur at the contraction inlet, at the throat inlet or in the

diffuser. Preliminary tests on the prototype venturi of Fig. 18 showed no evidence of any of the above mentioned phenomena, with the exception of intermittent rotating separation in the diffuser, a problem reported by Oldenziel as well [1]. In view of this, the boundary layer correlation parameter $\lambda = \theta^2 U' / \nu$ (where θ is the momentum thickness, U' is the streamwise derivative of the boundary layer edge velocity and ν is the kinematic viscosity) and the Stratford laminar boundary layer separation criterion, S_c , [12] have been plotted in Fig. 22. Separation is predicted when $\lambda = -.09$ or $S_c = 0$. The two methods agree well with each other and also with the observed location of separation in the prototype venturi, thus indicating that less steep diffusers should be used.

SUMMARY AND CONCLUSIONS

The operation of C.S.M.'s has been analyzed in order to investigate the possibility of extending their use to determine the concentration of unstable cavitation nuclei in a liquid as a function of the applied tension, from which the nuclei number distribution can be deduced.

By means of various assumptions and approximations, a simplified model has been derived which adequately represents the operation of C.S.M.'s in terms of a limited number of relevant parameters. The investigation of their mutual relations led to a functional description of C.S.M. operation which enables one to address the problem of their design in a systematic and organic way.

The above model has been applied to simulate C.S.M. operation for the case of a typical nuclei number distribution in water. The results can be

summarized as follows:

- a) the pressure in the C.S.M. cavitation region is an extremely sensitive parameter and cannot be measured directly with the necessary accuracy;
- b) the indirect measurement of the pressure in the cavitation region is best accomplished by the measurement of the potential core velocity at the C.S.M. throat by means of a L.D.V.;
- c) the existence of a potential core at the throat has been demonstrated by estimating boundary layer effects;
- d) for the specific nuclei number distribution considered, the errors and limitations due to saturation can be reduced by appropriately decreasing the volume of the cavitation region;
- e) the time response of the cavitating nuclei imposes a lower bound for the length of the C.S.M. throat section;
- f) the flow can sustain without separation or fluid mechanical instabilities the very large and steep contraction suggested by design considerations, but is extremely sensitive to separation in the diffuser;
- g) in the case of the nuclei number distribution used as an example, it appears that C.S.M.'s can be designed which are capable of detecting gas bubbles having an equilibrium radius larger than about 10 μm within the errors typical of other alternative techniques currently available;
- h) due to the considerable complexity of the phenomena involved, the interpretation of the data obtained from C.S.M.'s requires a careful analysis.

ACKNOWLEDGEMENT

The authors would like to thank Carol Kirsch for her help in organizing this manuscript. This work was supported by Naval Sea Systems Command General Hydromechanics Research Program Administered by the David Taylor Naval Ship Research and Development Center under Contract No. N00014-75-C-0378.

REFERENCES

1. Oldenziel, D. M., "A new instrument in cavitation research: the cavitation susceptibility meter", ASME Journal of Fluids Engineering, 104, June 1982, pp. 136-142.
2. Oldenziel, D. M., Jansen, R. H. J., Keller, A. P., Lecoffre, Y., and van Renesse, R. L., "Comparison of instruments for detection of particles and bubbles in water during cavitation studies", Proceedings of Symposium on Operating Problems of Pump Stations and Power Plants, IAHR, Amsterdam, September 1982.
3. Oldenziel, D. M., "Utility of available instruments during cavitation tests", Proceedings of Symposium on Operating Problems of Pump Stations and Power Plants, IAHR, Amsterdam, September 1982.
4. Godefroy, H. W. H. E., Jansen, R. H. J., Keller, A. P., and van Renesse, R. L., "Comparison of measuring and control methods of the water quality with respect to cavitation behaviour", Delft Hydraulics Laboratory Publication, January 1981.
5. Knapp, R. T., Daly, J. W. and Hammit, F. G., "Cavitation", McGraw Hill, 1970.
6. van Wijngaarden, L., 1972, "One-dimensional flow of liquids containing small gas bubbles", Ann. Rev. Fluid Mech., Vol. 4, pp.369-396.
7. Plesset, M.S. and Prosperetti, A., "Bubble dynamics and cavitation", Ann. Rev. Fluid Mech., 1977, Vol. 9, 145-85.

8. Chmielewski, G. E., "Boundary layer consideration in the design of aerodynamic contractions", J. of Aircraft, Vol. 11, No. 8, August 1974, pp. 435-438.
9. Mikhail, M. N., "Optimum design of wind tunnel contractions", AIAA Journal, Vol. 17, No. 5, May 1978, pp. 471-477.
10. White, F. M., "Viscous fluid flow", Mc Graw Hill, 1974.
11. Brownlee, K. A., "Statistical theory and methodology in science and engineering", John Wiley & Sons, 1960.
12. Stratford, B. S., "Flow in laminar boundary layer near separation", Aeronautical Research Council, R&M 3002, November 1954.
13. Le Goff, J. P. and Lecoffre, Y., "Nuclei and cavitation", 14th. Symposium on Naval Hydrodynamics, National Academy Press, 1983, pp. 215-242.

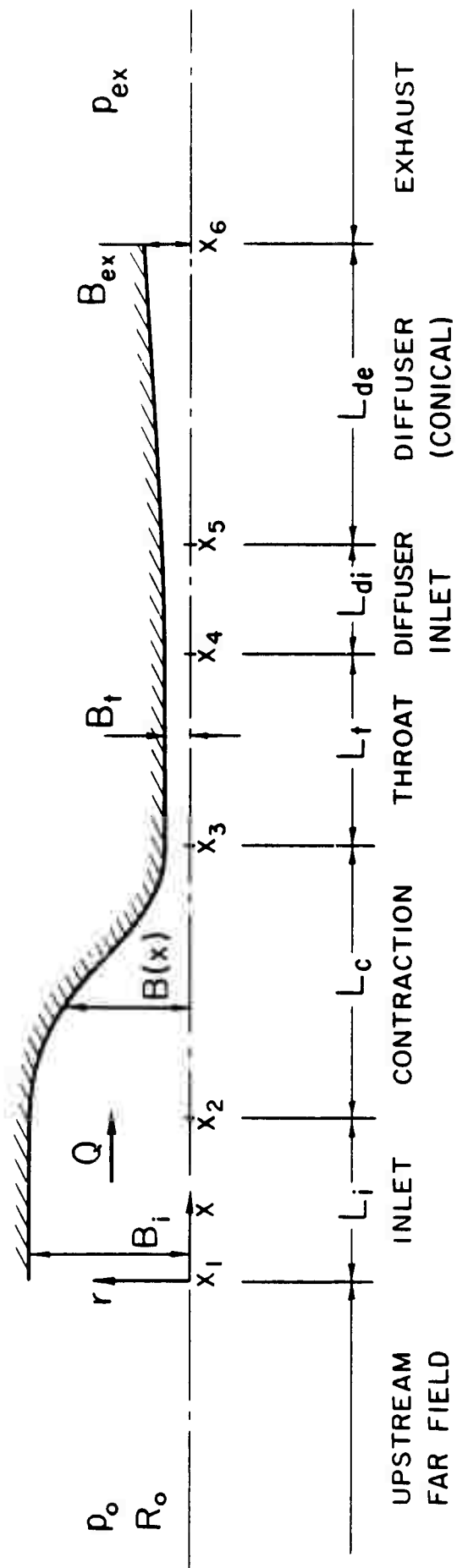


Figure 1. Axisymmetric duct geometry and nomenclature.

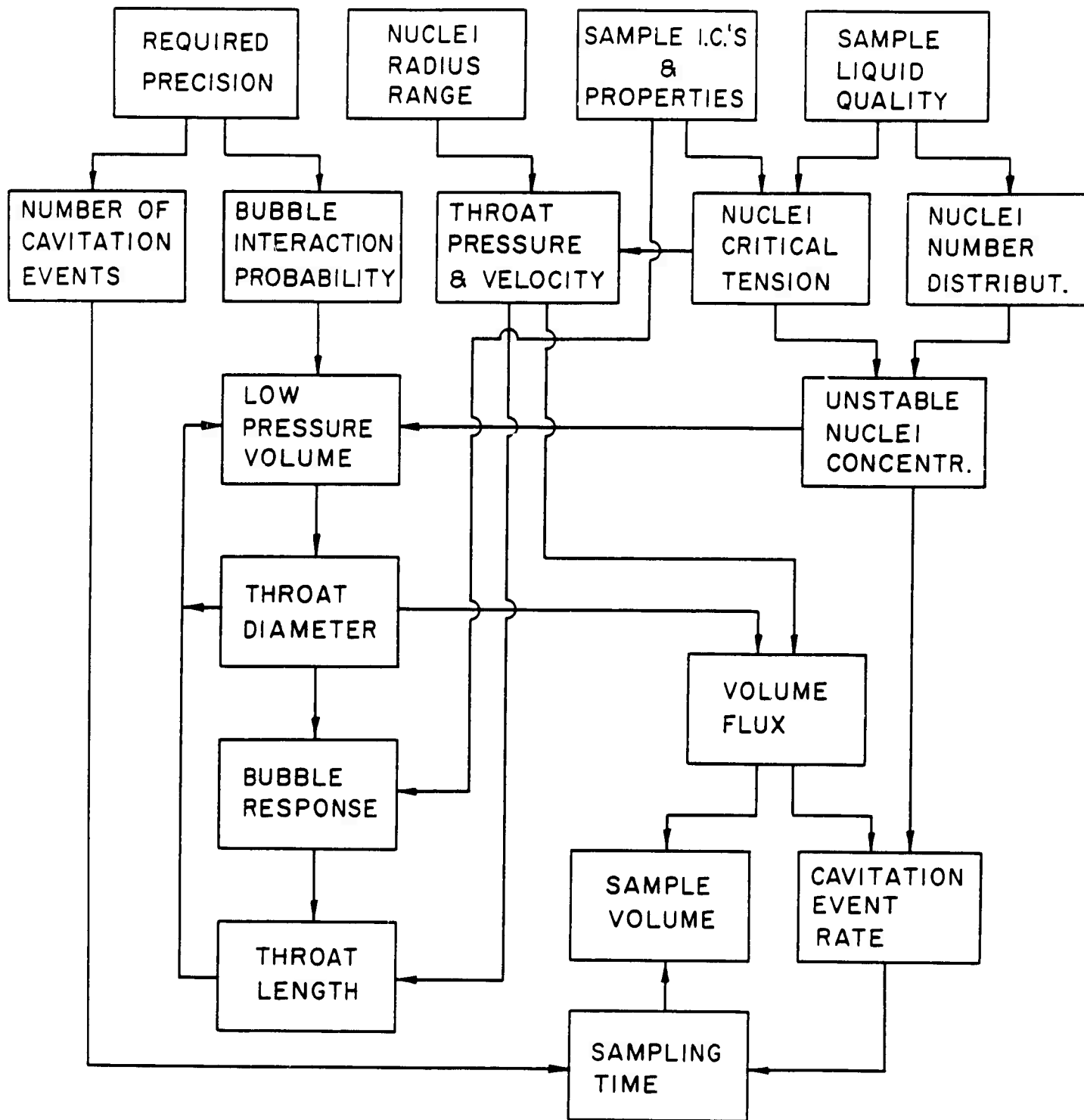
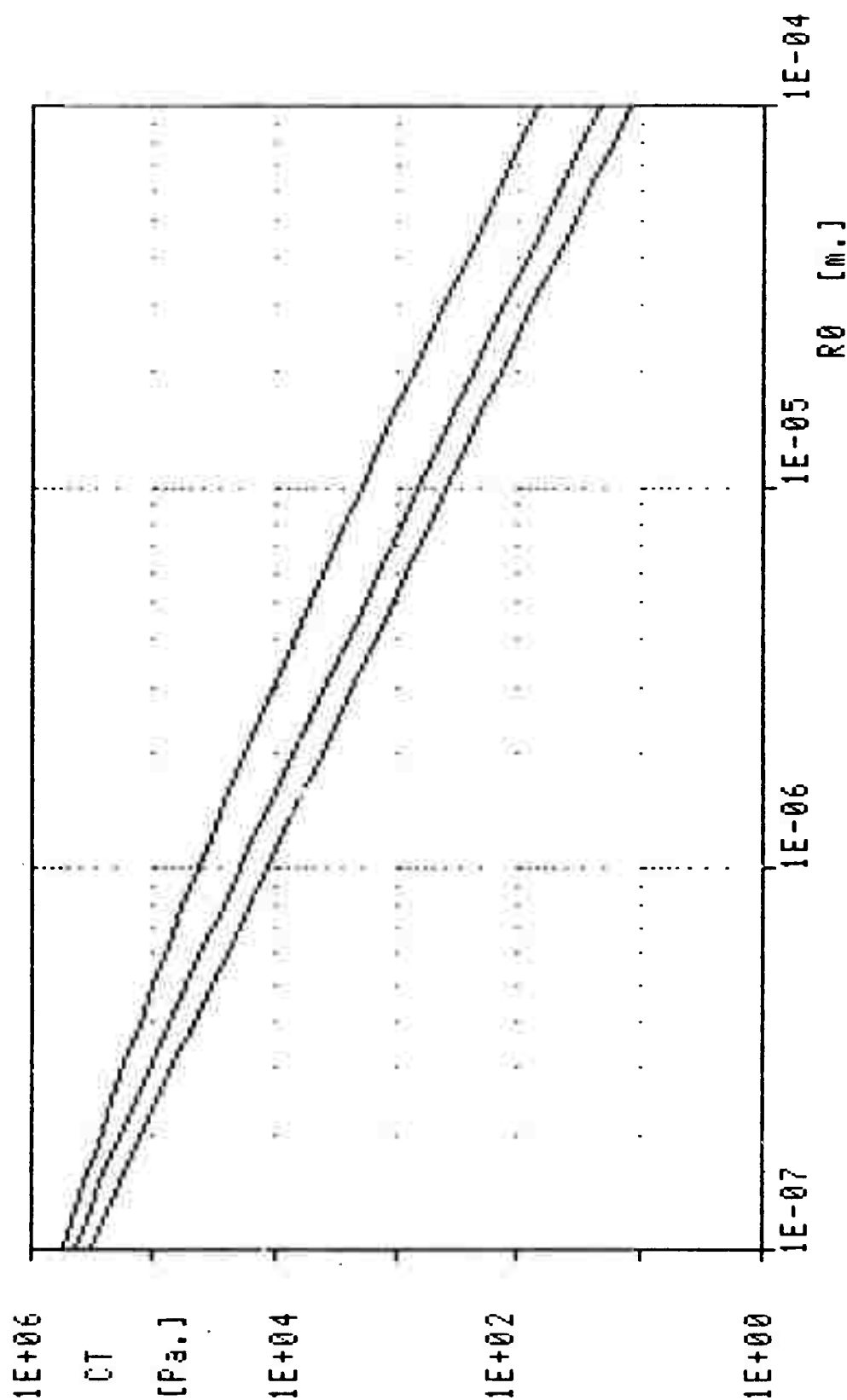
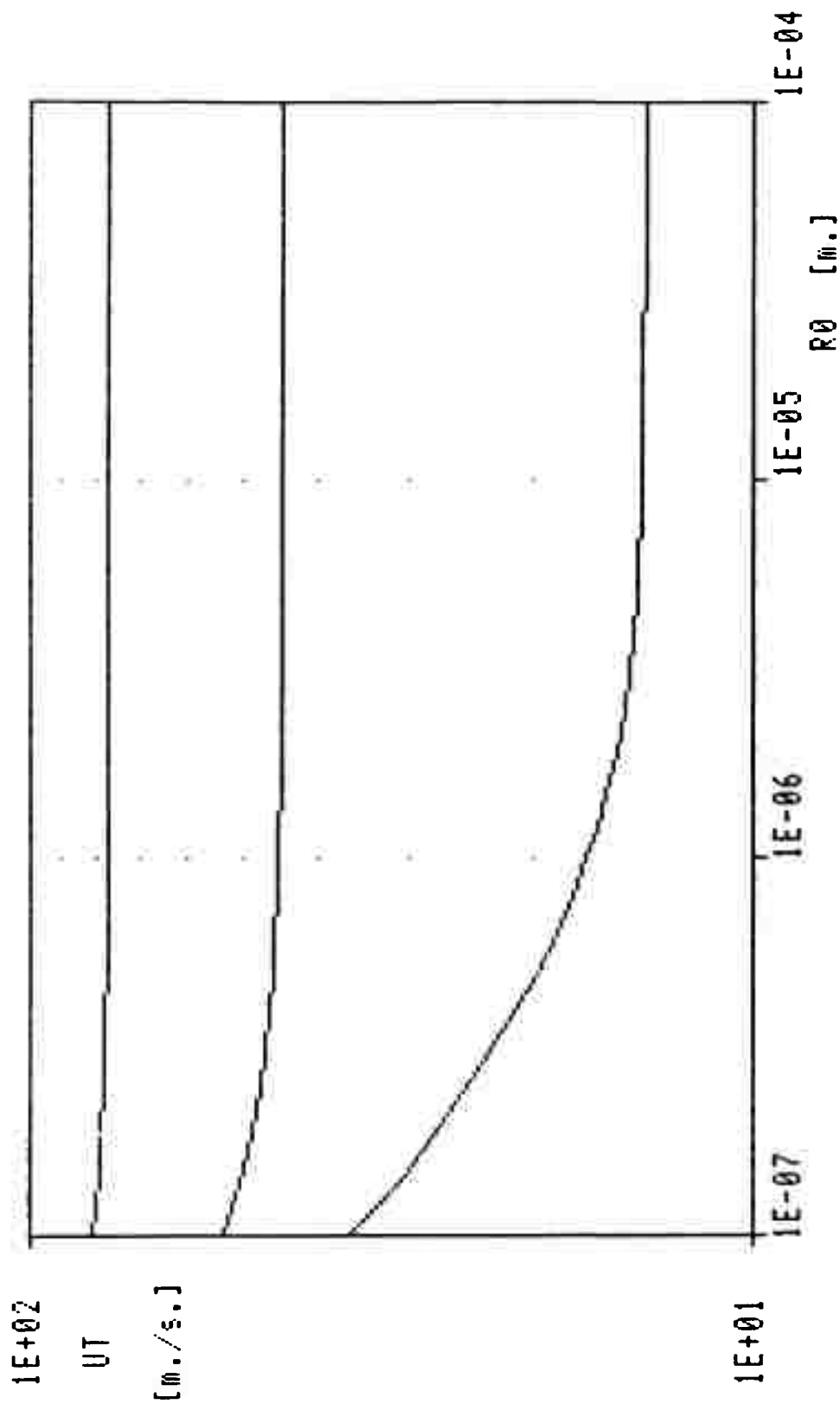


Figure 2. Block diagram showing the main parameters of C.S.R.'s and their mutual relations.



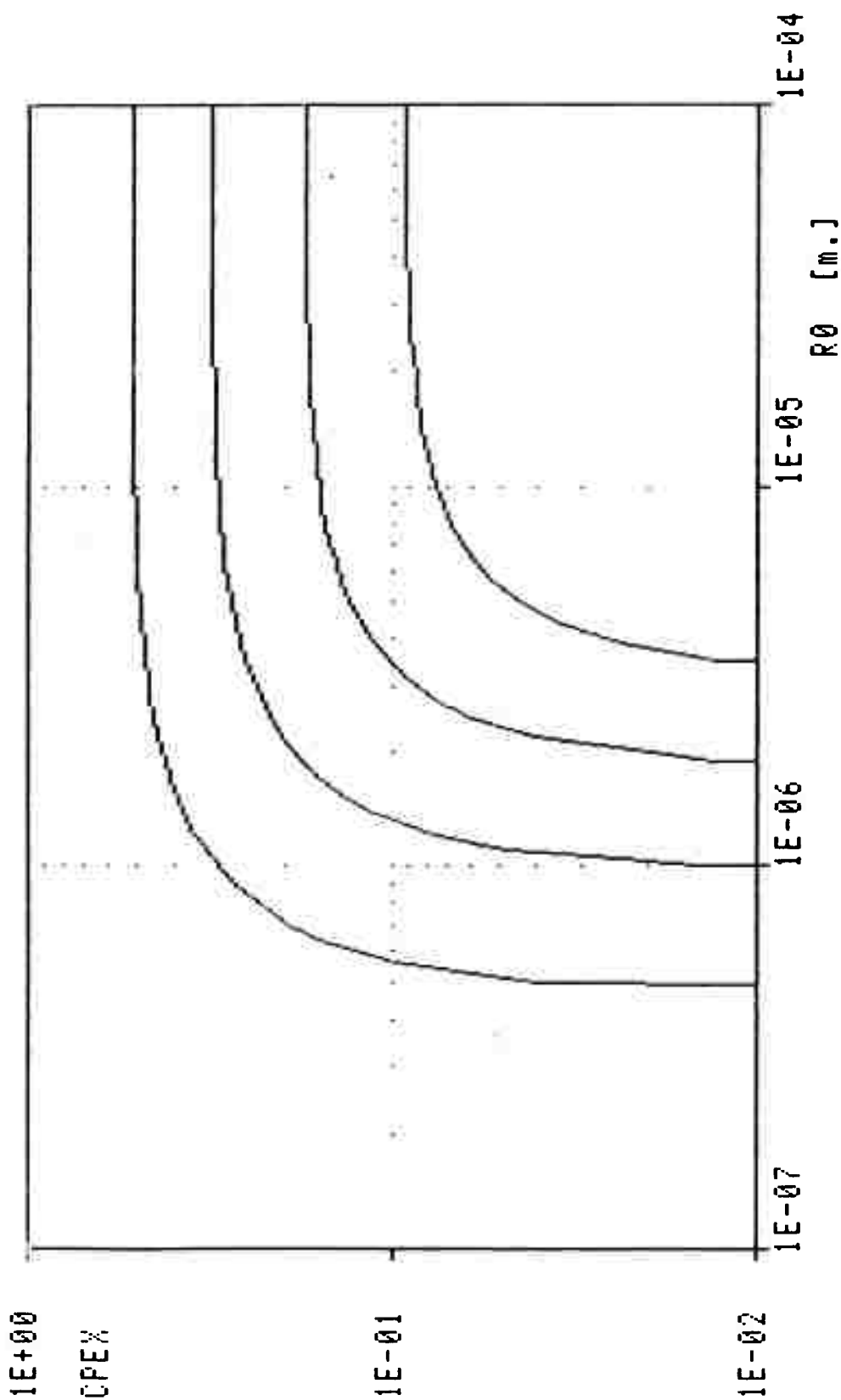
CRITICAL TENSION, CT, V/S BUBBLE EQUILIBRIUM RADIUS, R0

Figure 3. Critical tension, $(p_v - p)_{cf}$ [CT], of isolated spherical bubbles in an unbounded liquid as function of their static equilibrium radius, R_0 [R0], at various equilibrium pressures: $p_0 = 1$ bar (upper curve), $p_0 = 10$ bar (intermediate curve) and $p_0 = 30$ bar (lower curve) for water - air at $T = 20$ °C (surface tension $S = .073$ N/m and vapor pressure $p_v = 1919$ Pa).



CRITICAL THROAT VELOCITY, u_t , V/S EQUILIBRIUM RADIUS, R_0

Figure 4. Throat velocity, u_t [UT], v/s bubble equilibrium radius, R_0 [R0], at various equilibrium pressures: $p_0 = 1$ bar (lower curve), $p_0 = 10$ bar (intermediate curve) and $p_0 = 30$ bar (upper curve) for $S = .073$ N/m (surface tension), $p_v = 1919$ Pa (vapor pressure) and $\rho = 1000$ kg/m³ (liquid density).



EXHAUST PRESSURE COEFFICIENT, CPEX, V/S EQUILIBRIUM BUBBLE RADIUS, R0

Figure 5. Exhaust pressure coefficient, C_{peX} [CPEX], v/s bubble equilibrium radius, R_0 [R0], at $p = 1$ bar and for exhaust to throat diameter ratio: $D_{ex}/D_t = 1.025, 1.058, 1.100$ and 1.200 from the lower to the upper curve respectively. Here: $C_{peX} = (p_{ex} - p_v) / (p_o - p_v)$, where p_{ex} is the exhaust pressure. The curves shift to the left at higher values of p_o .

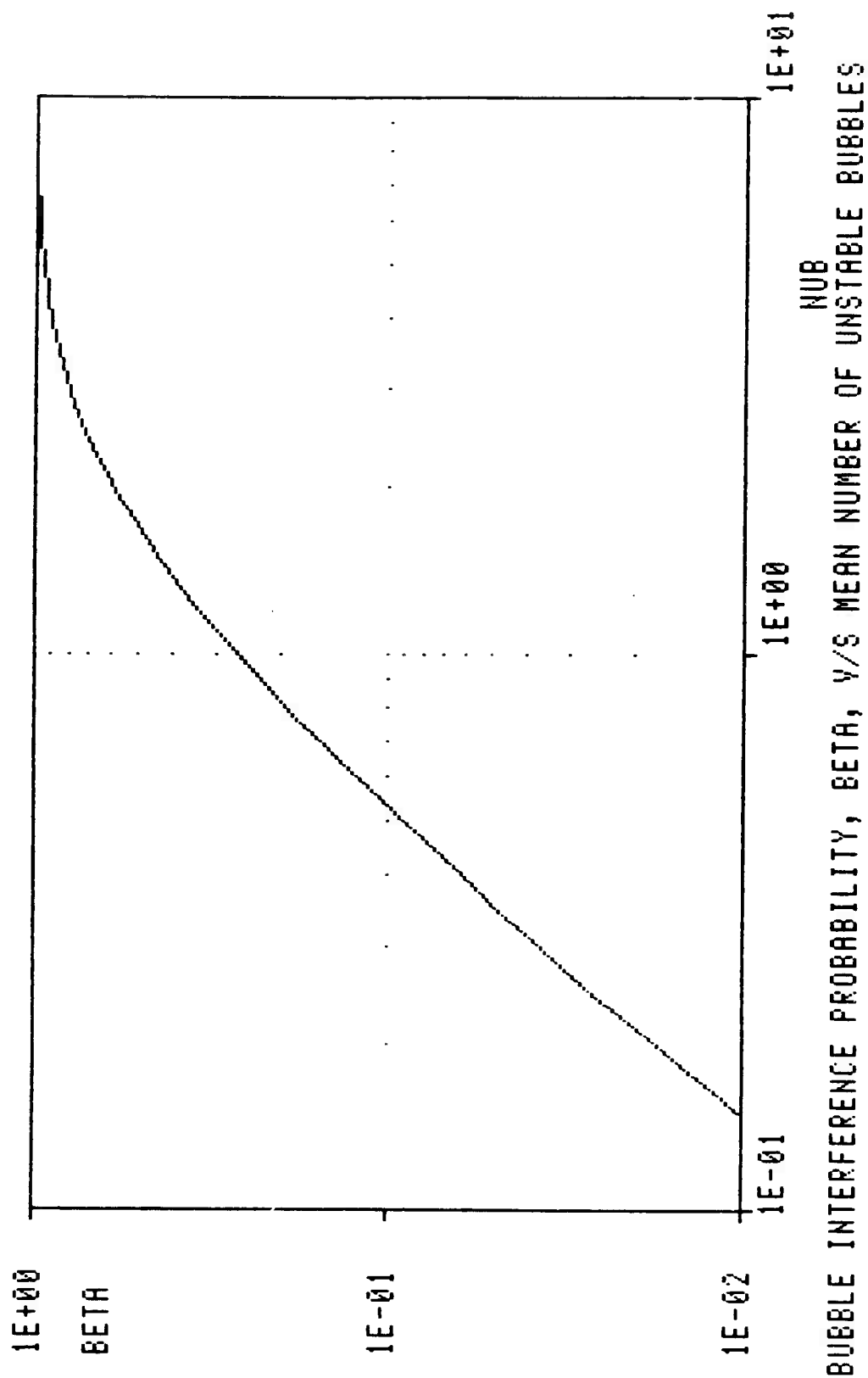
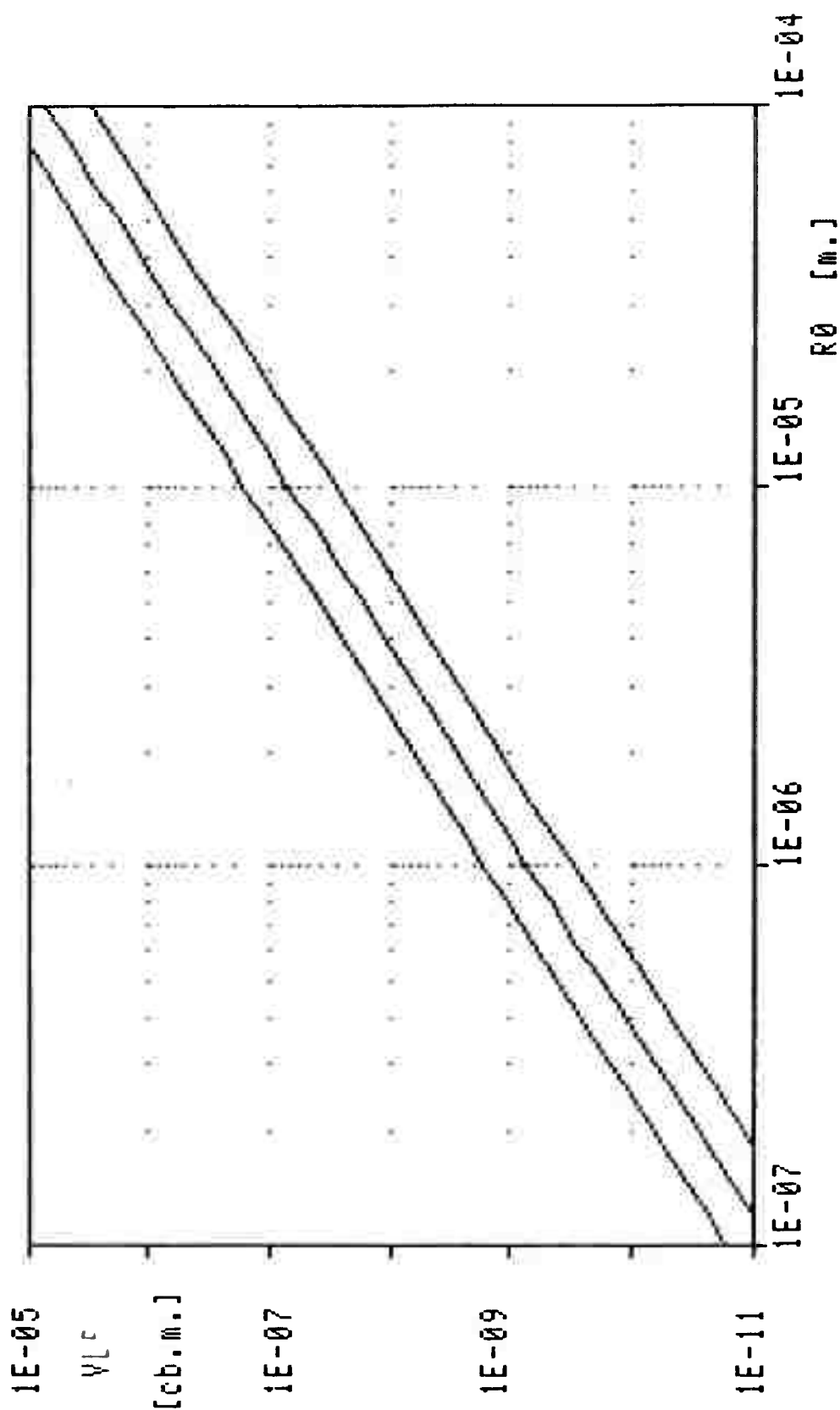
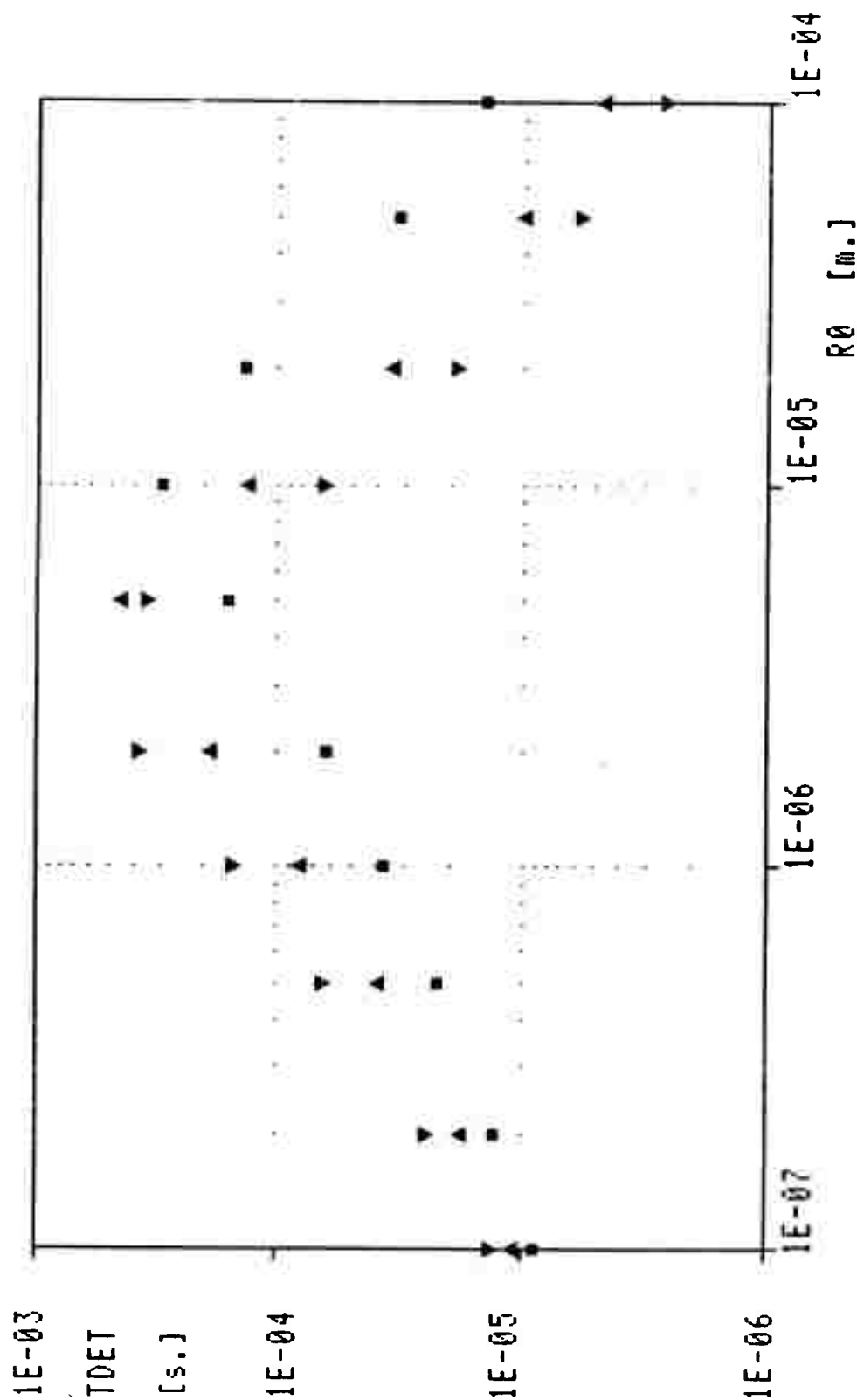


Figure 6. Bubble interference probability, β [BETA], i.e. probability of finding more than one bubble in the cavitation region of the duct, v/s the average number of unstable bubbles in the same region, N_{ub} [NUB]. Such probabilities are calculated assuming that the occurrence of cavitation nuclei in a given volume is represented by a Poisson process.



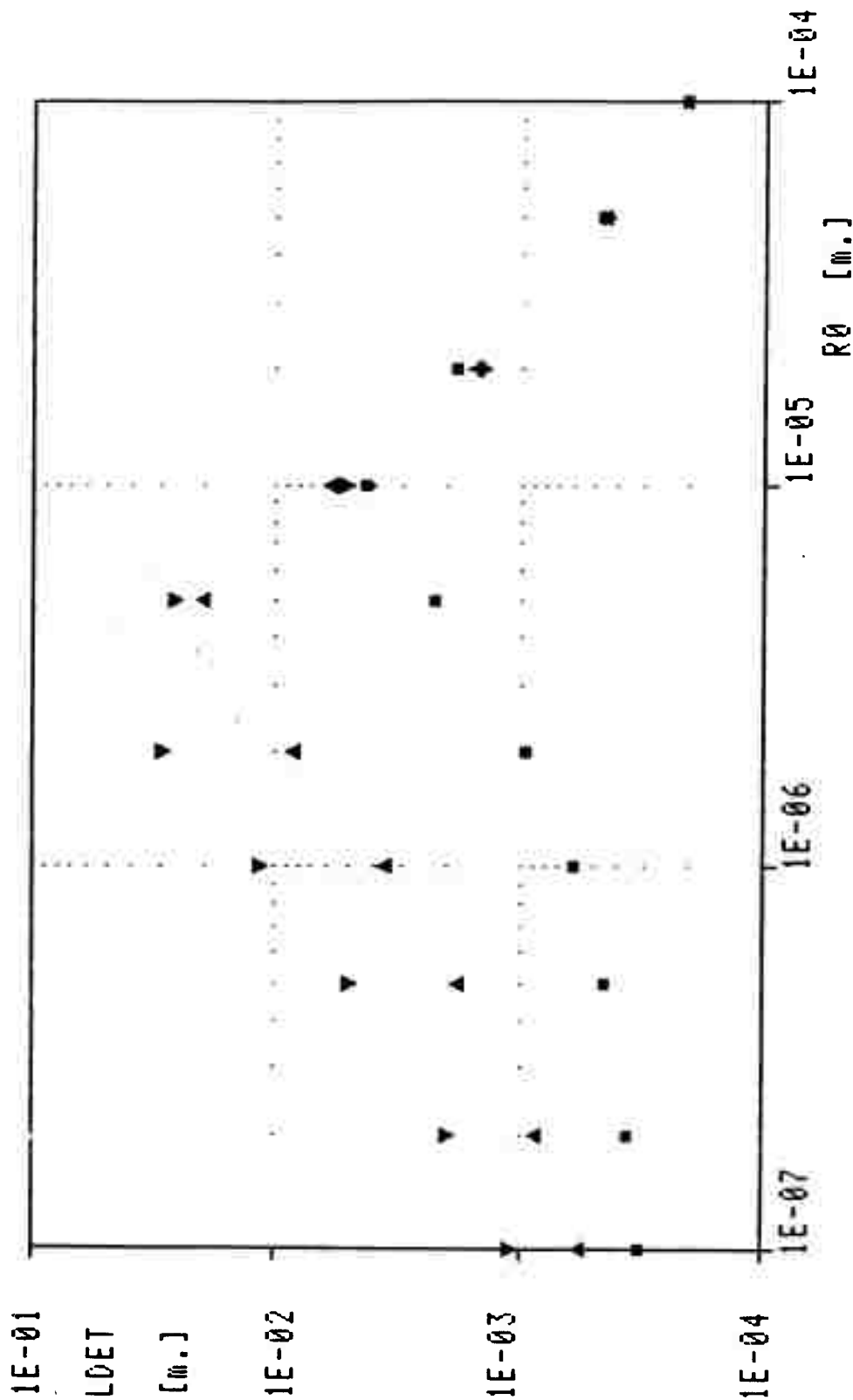
LOW PRESSURE VOLUME, VLP, V/S BUBBLE EQUILIBRIUM RADIUS, R_0

Figure 7. Low pressure volume of the duct, V_{LP} [VLP], v/s bubble equilibrium radius, R_0 [R0], for $K_{dis} = .001$ 1/m (nuclei number distribution parameter) and various average numbers of unstable bubbles in such a volume: $N_{ub} = .1486$ (lower curve), .3554 (intermediate curve), and .8244 (upper curve). The corresponding values of the bubble interference probability are: $\beta = .01$, .05 and .20.



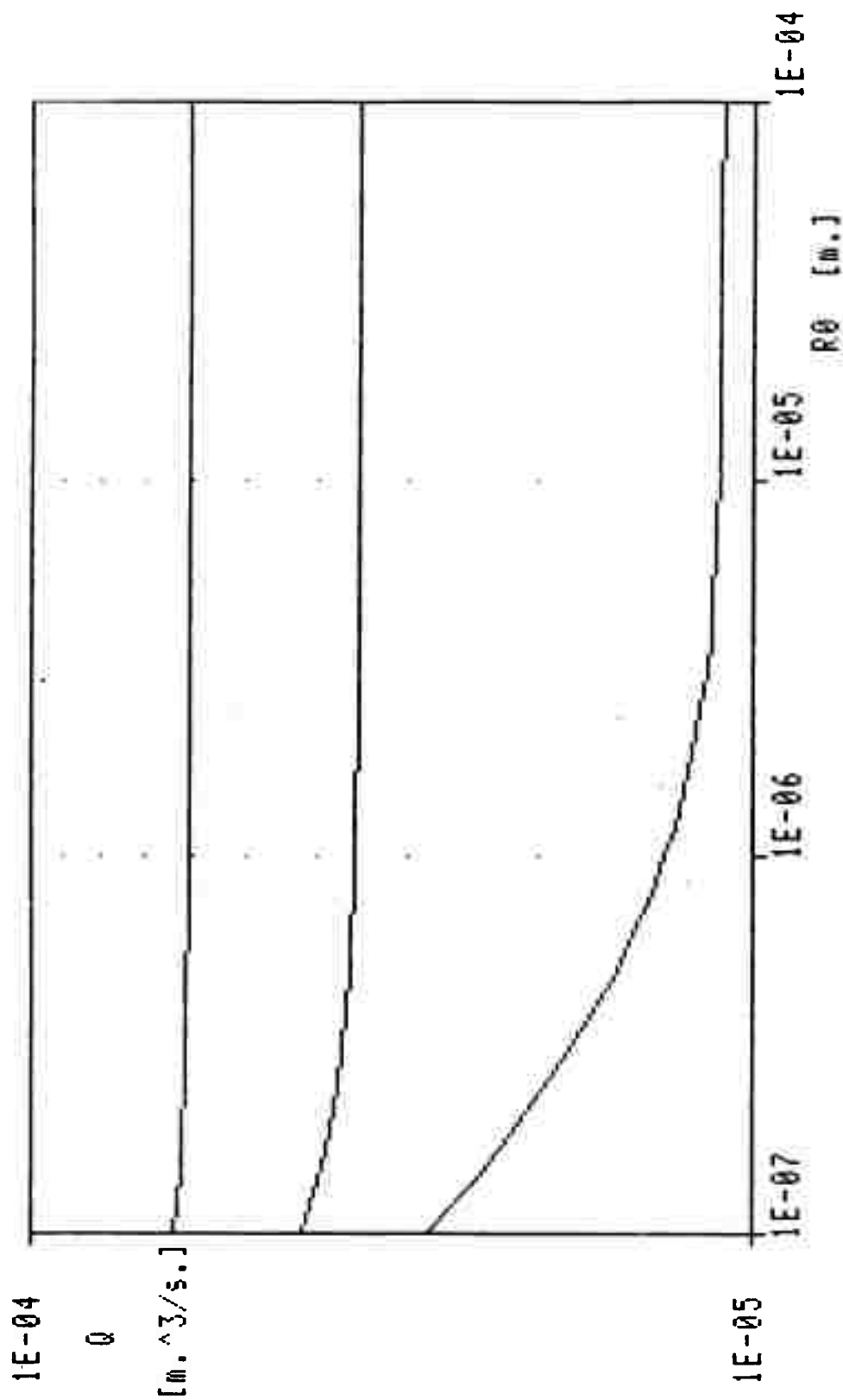
DETECTION TIME, T_{DET} , V/S EQUILIBRIUM BUBBLE RADIUS, R_0

Figure 8. Bubble detection time, T_{DET} , i.e. time necessary for a bubble to reach a detectable radius size, R_{det} , v/s equilibrium bubble radius, R_0 , for various bubble equilibrium pressures: $p = 1$ bar (squares), 10 bar (upward triangles) and 30 bar (downward triangles). Here: $R_{det} = .150$ mm, $p_v = 1919$ Pa (vapor pressure), $S = .073$ N/m (surface tension), $\rho = 1000$ kg/m³ (liquid density) and $D_t = 1$ mm (throat diameter). The data are obtained from the numerical solution of the unsteady one-dimensional ideal flow generated by the growth of a single spherical bubble in a semi-infinite cylindrical duct, whose unperturbed steady pressure is equal to the bubble critical pressure.



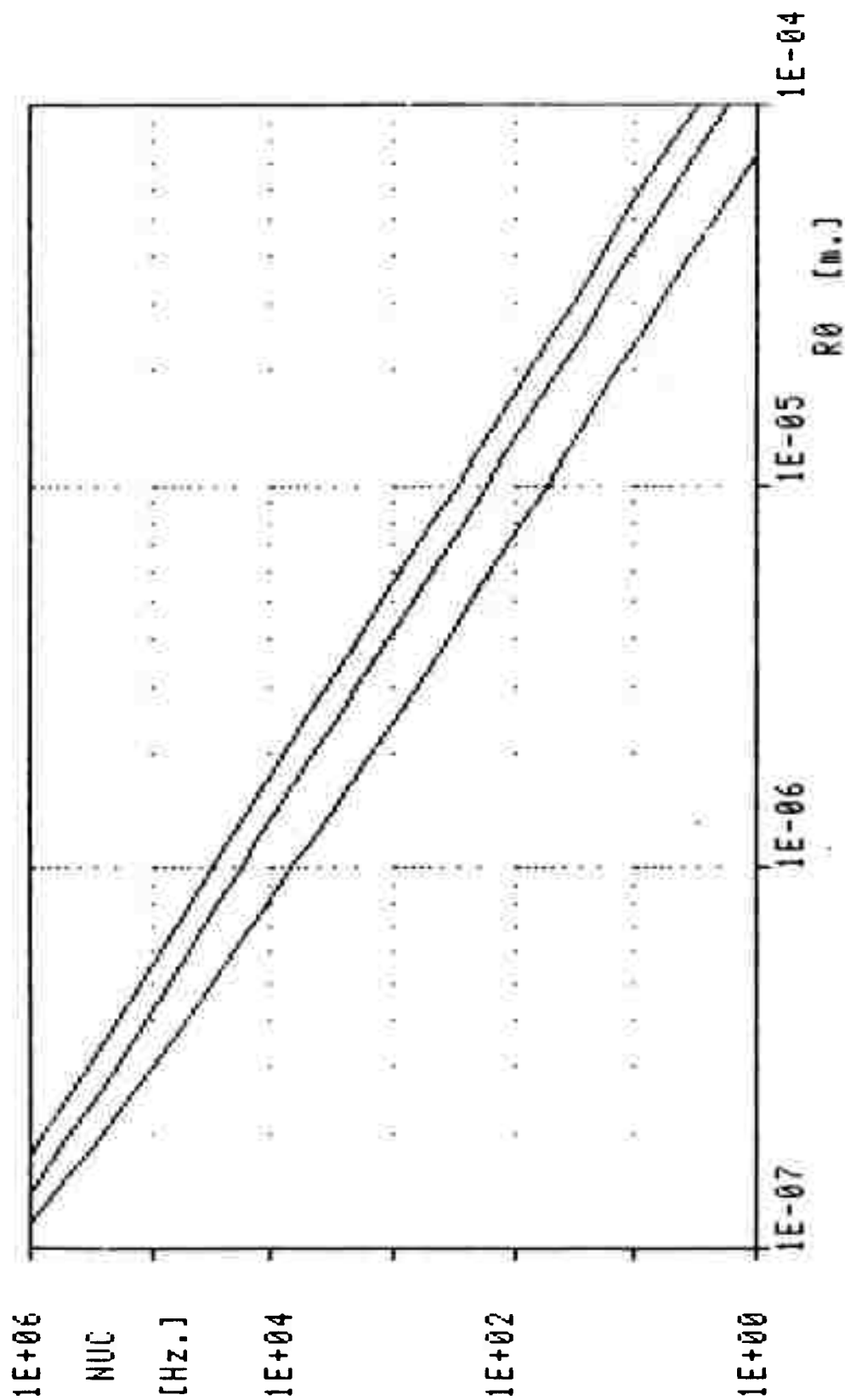
DETECTION LENGTH, LDET, V/S EQUILIBRIUM BUBBLE RADIUS, R0

Figure 9. Bubble detection length, L_{det} [LDET], i.e. length necessary for a bubble to reach a detectable radius size, R_{det} , v/s equilibrium bubble radius R_0 [R0], for various bubble equilibrium pressures: $P_0 = 1$ bar (squares), 10 bar (upward triangles) and 30 bar (downward triangles). Here: $R_{det} = 150$ μm , $P_v = 1919$ Pa (vapor pressure), $S = .073$ N/m (surface tension), $\rho = 1000$ kg/m³ (liquid density) and $D_t = 1$ mm (throat diameter). The data are obtained from the numerical solution of the unsteady one-dimensional ideal flow generated by the growth of a single spherical bubble in a semi-infinite cylindrical duct, whose unperturbed steady pressure is equal to the bubble



VOLUME FLOW RATE, Q , V/S BUBBLE EQUILIBRIUM RADIUS, R_0

Figure 10. Volume flow rate, Q , v/s equilibrium bubble radius, R_0 [R0], at various equilibrium pressures: $p_0 = 1 \text{ bar}$ (lower curve), $p_0 = 10 \text{ bar}$ (intermediate curve) and $p_0 = 30 \text{ bar}$ (upper curve) for $S = .073 \text{ N/m}$ (surface tension), $p_v = 1919 \text{ Pa}$ (vapor pressure), $\rho = 1000 \text{ kg/m}^3$ (liquid density) and $D_t = 1 \text{ mm}$ (throat diameter).



MEAN CAVITATION EVENT RATE, NUC , V/S BUBBLE EQUILIBRIUM RADIUS, R_0

Figure 11. Mean cavitation event rate, V [NUC], v/s bubble equilibrium radius, R_0 [R0], for various bubble equilibrium pressures: $p_0 = 1$ bar (lower curve), 10 bar (intermediate curve) and 30 bar (upper curve). Here: $D_t = 1$ mm (throat diameter), $p_3 = 1919$ Pa (vapor pressure), $S = .073$ N/m (surface tension), $\rho = 1000$ kg/m³ (liquid density) and $K_{dis} = .001$ 1/m (nuclei number distribution parameter).

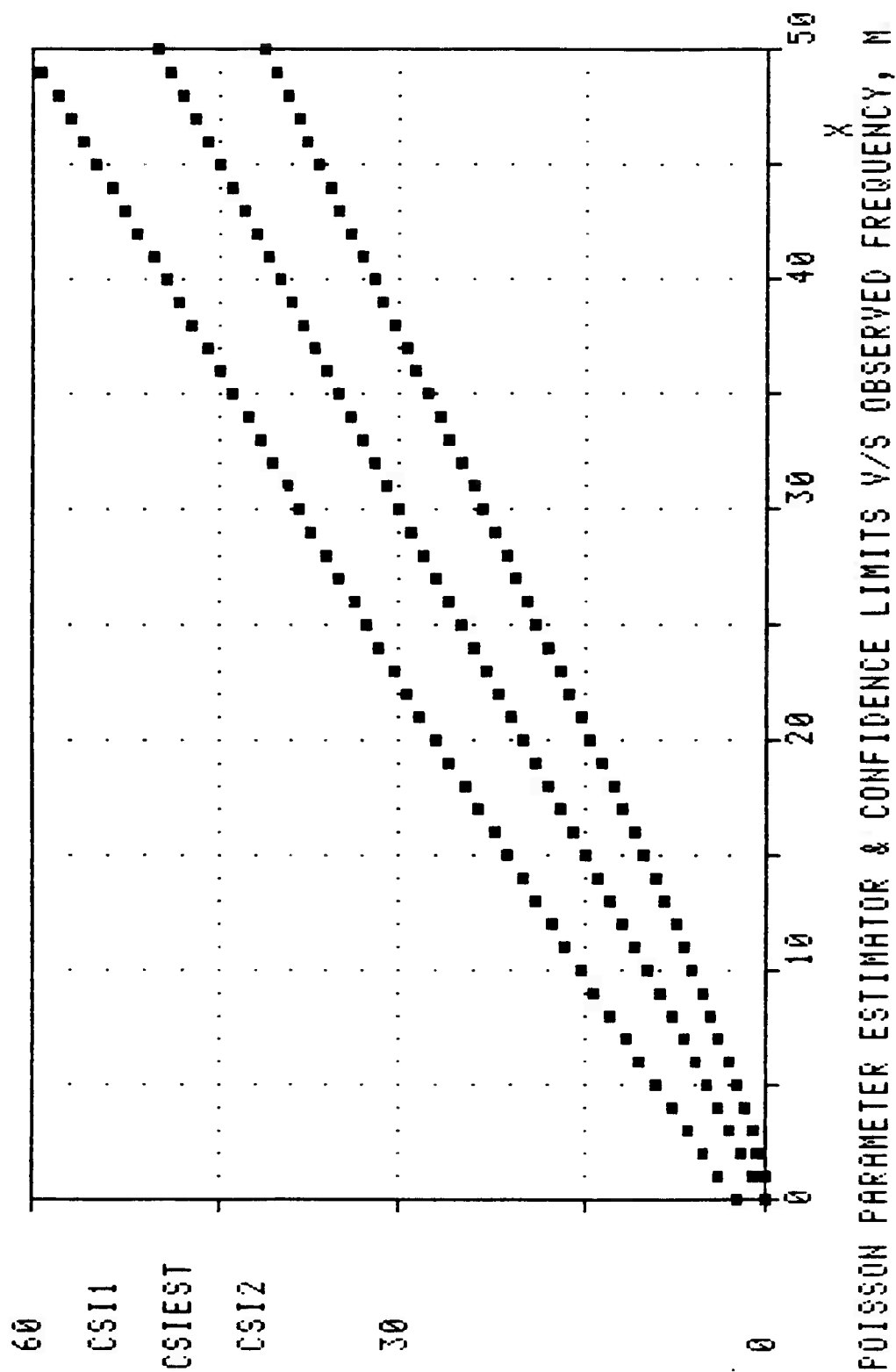
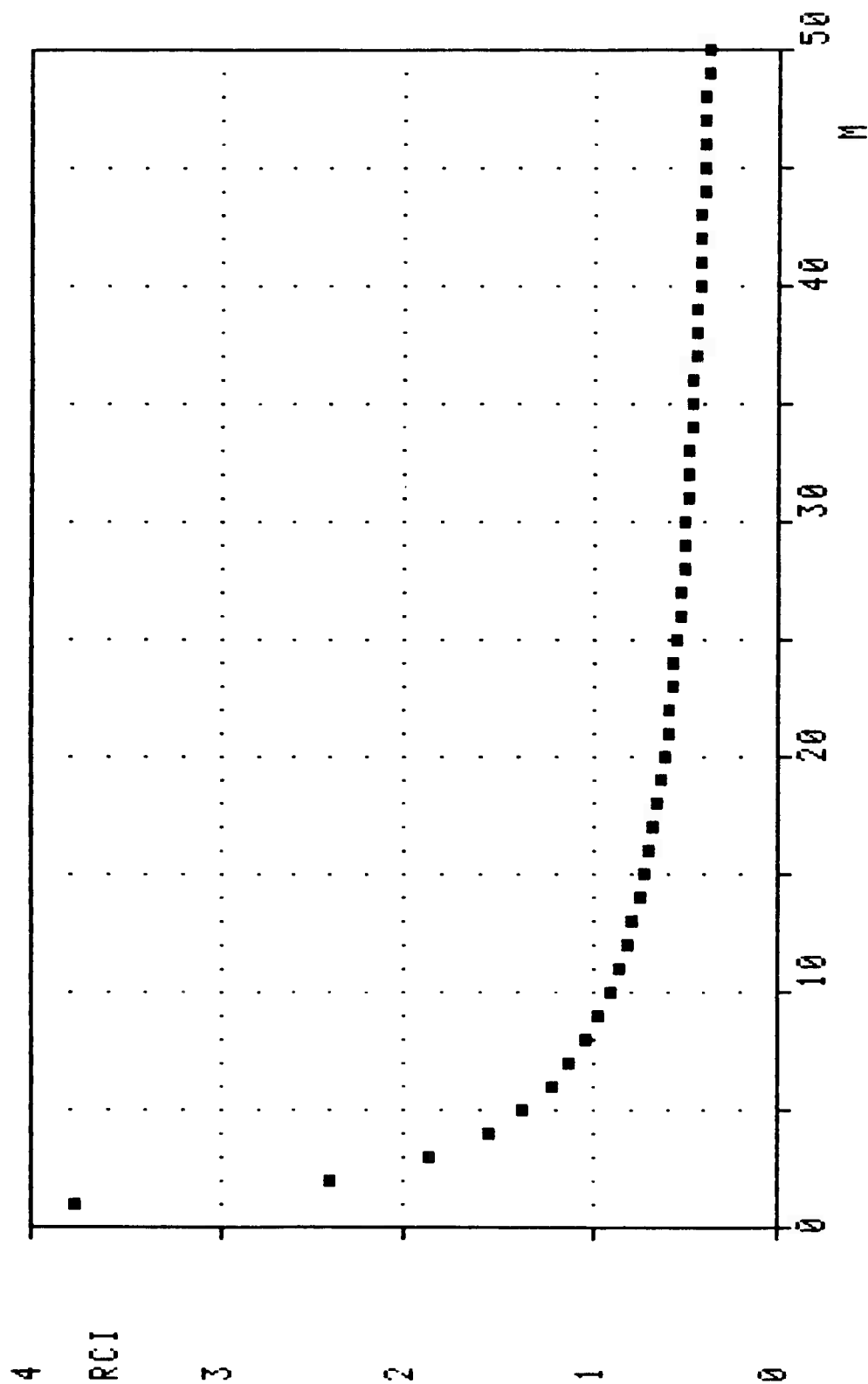


Figure 12. Poisson's distribution parameter estimator, ξ_{est} [CS1EST], and confidence limits, ξ_1 [CS11] and ξ_2 [CS12], v/s sample statistical frequency, m [M]. Here the confidence level is: $1 - \alpha = .8$.



RELATIVE CONFIDENCE INTERVAL, RCI, χ^2/ν OBSERVED FREQUENCY, M

Figure 13. Poisson's distribution parameter relative confidence interval, $(\xi_2 - \xi_1)/m$ [RCI], χ^2/ν sample statistical frequency, m [M]. Here the confidence level is: $1 - \alpha = .8$ and the confidence interval is normalized w.r.t. the sample frequency.

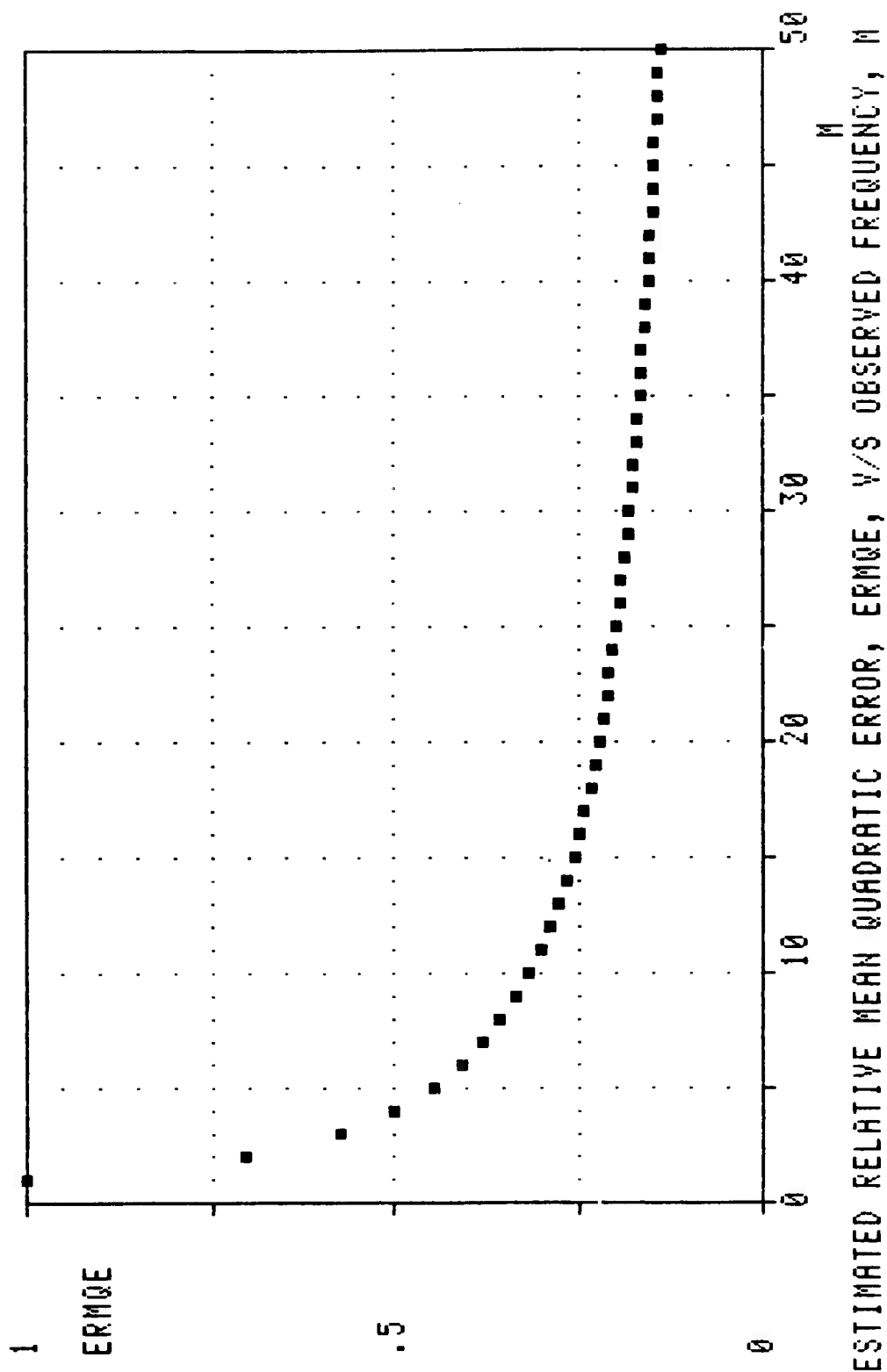
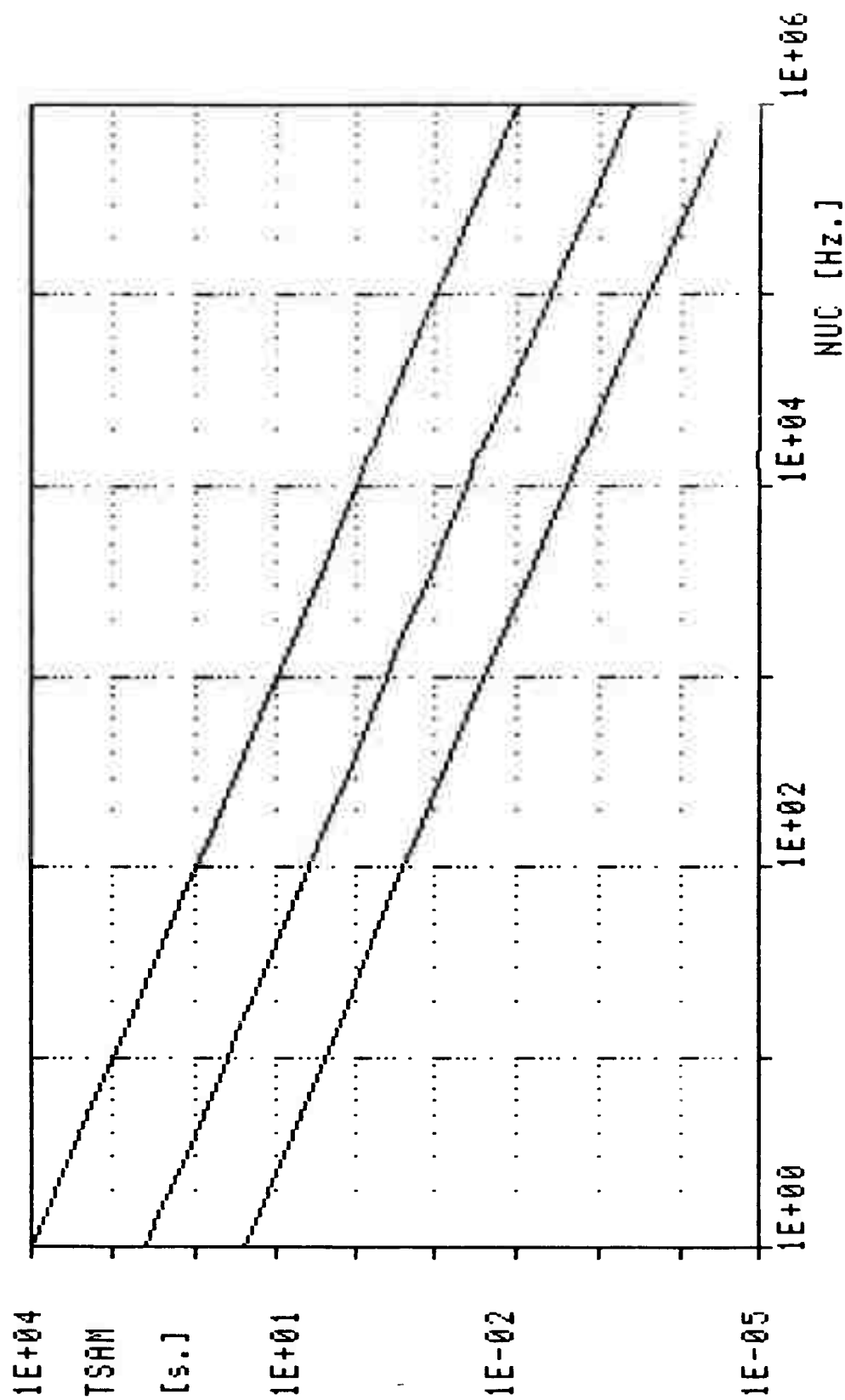


Figure 14. Poisson's distribution parameter estimated relative mean quadratic error, s [ERMQE], v/s sample statistical frequency m [M]. Here the best estimator of the Poisson's distribution parameter (the sample frequency) is used to both evaluate the r.m.s. error and to normalize it.



SAMPLING TIME, TSAM, V/S MEAN CAVITATION EVENT FREQUENCY, NUC

Figure 15. Sampling time, T [TSAM], v/s average cavitation event rate, V_c [NUC], for various values of the relative estimated r.m.s. error: $\epsilon = 0.1$ (upper curve), .05 (intermediate curve) and .20 (lower curve).

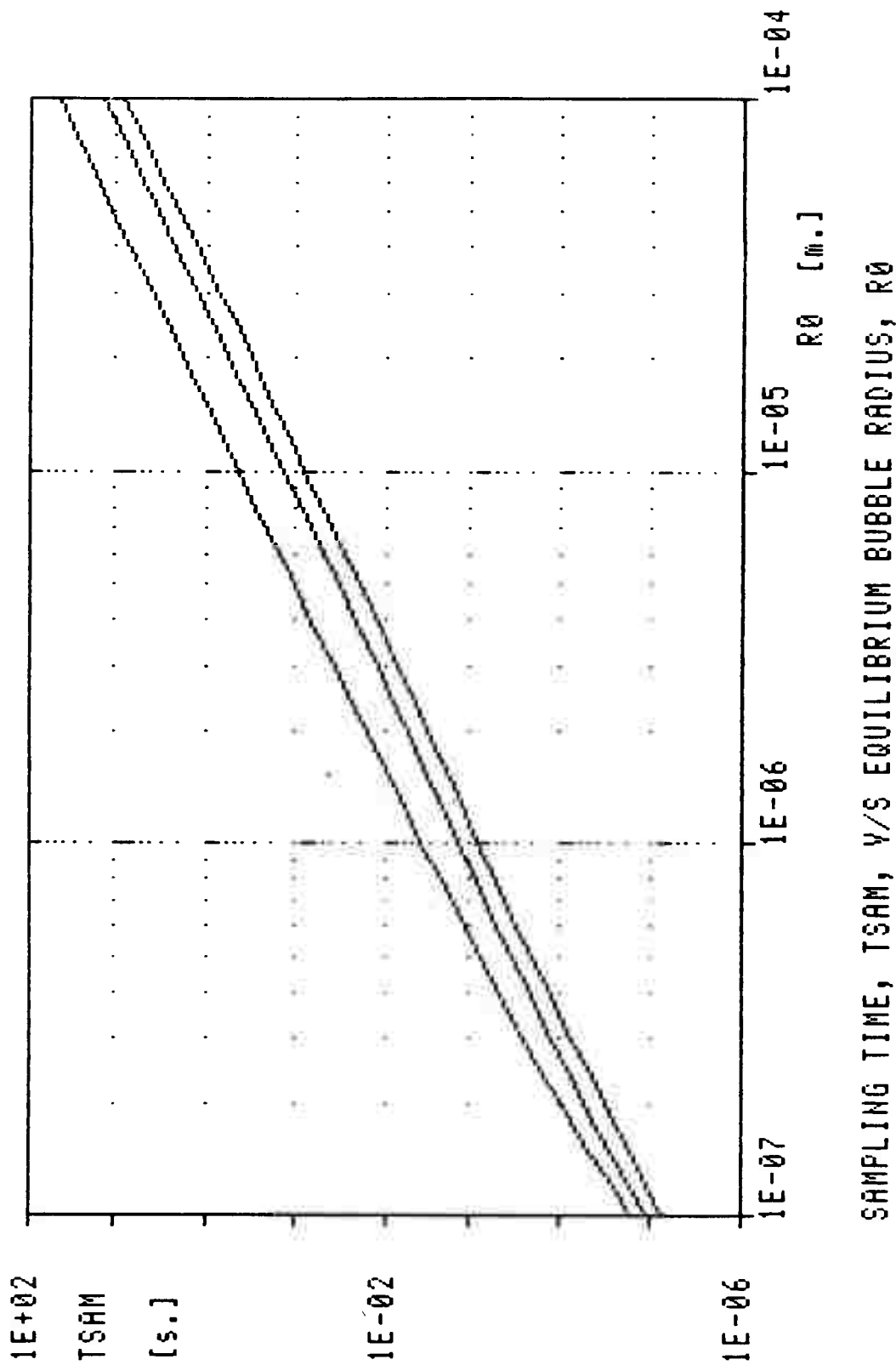


Figure 16. Sampling time T [TSAM], v/s bubble equilibrium radius, R_0 [R_0], for various values of the bubble equilibrium pressure: $p_0 = 1$ bar (upper curve), 10 bar (intermediate curve) and 30 bar (lower curve). Here: $\epsilon = .20$ (estimated relative r.m.s. error in the measure of the cavitation event rate), $D_t = .001$ m (throat diameter), $p_v = 1919$ Pa (vapor pressure), $S = .073$ N/m (surface tension), $\rho = 1000$ kg/m³ (liquid density) and $K_{dis} = .001$ 1/m (nuclei number distribution parameter).

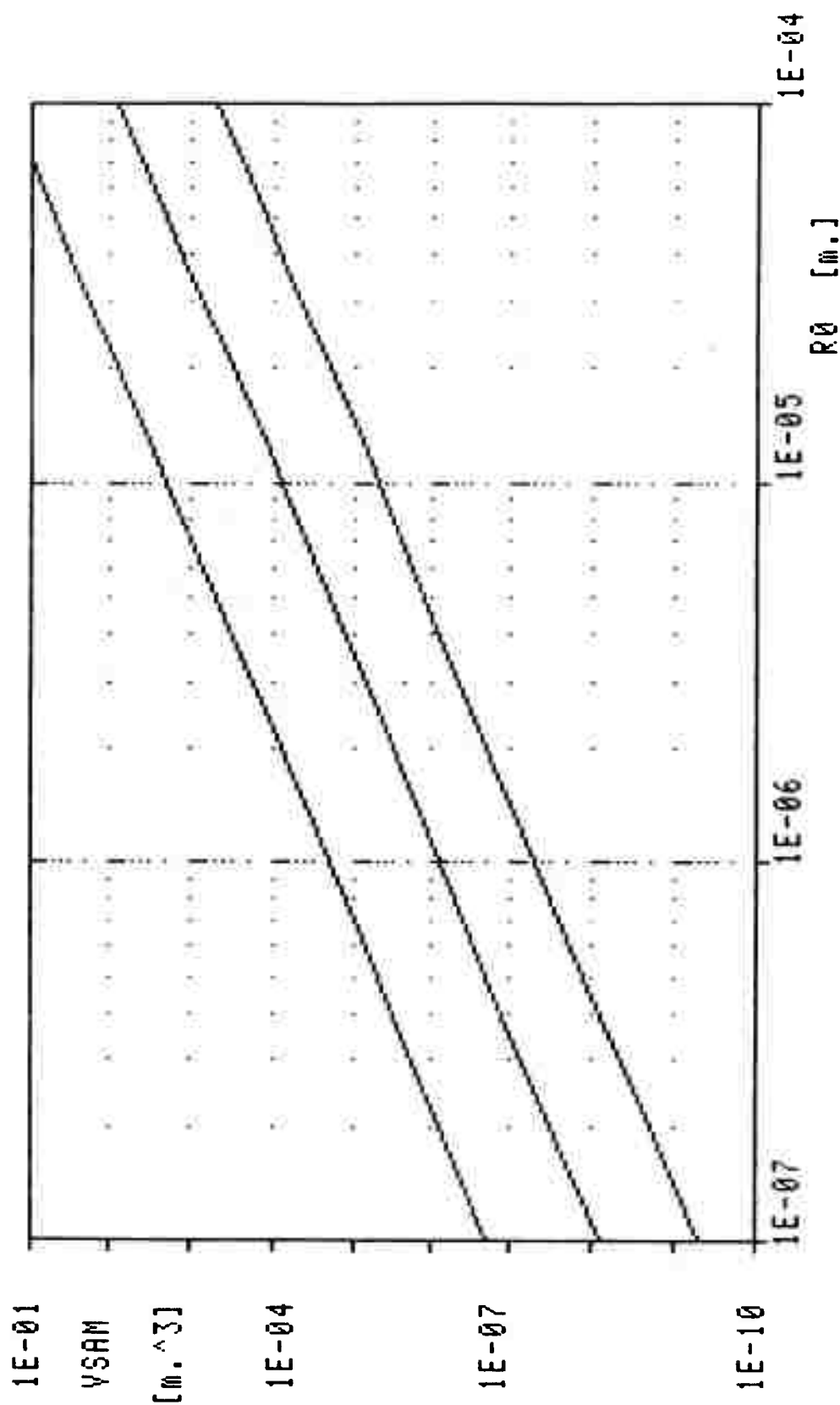
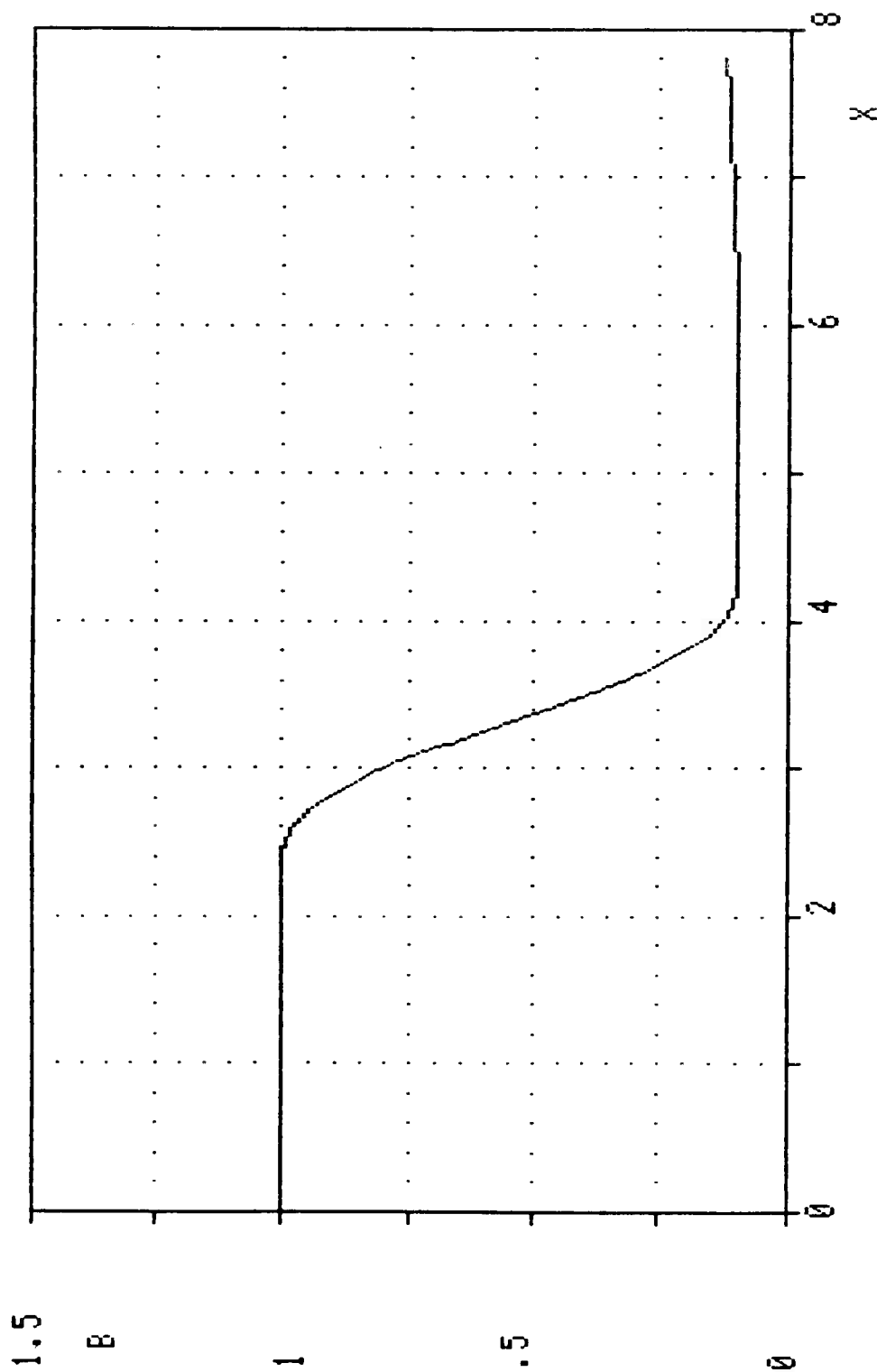


Figure 17. Liquid sample volume, V [VSAM], v/s bubble equilibrium radius, R_0 [R0], for various values of the estimated relative r.m.s. error in the measure of the cavitation event rate: $z = .01$ (upper curve), 0.85 (intermediate curve) and $.28$ (lower curve). Here: $K_{dis} = .001$ $1/m$ (nuclei number distribution parameter).



C.S.M. PROTOTYPE VENTURI DUCT RADIUS, $B(X)$, V/S AXIAL COORDINATE, X

Figure 18. Duct shape of prototype C.S.M. venturi in normalized coordinates X (axial) and B (radial) with: $C = 100$ (contraction ratio), $L_c = 2.278$ (normalized inlet length), $L_c = 2.076$ (normalized contraction length), $L_d = 1.544$ (normalized throat length), $L_{di} = .597$ (normalized diffuser inlet length), $L_{de} = 1.327$ (normalized conical diffuser length) and $\beta_d = .803$ deg (diffuser semi-aperture angle). Lengths are normalized w.r.t. the duct inlet radius, $B_i = 5$ mm.

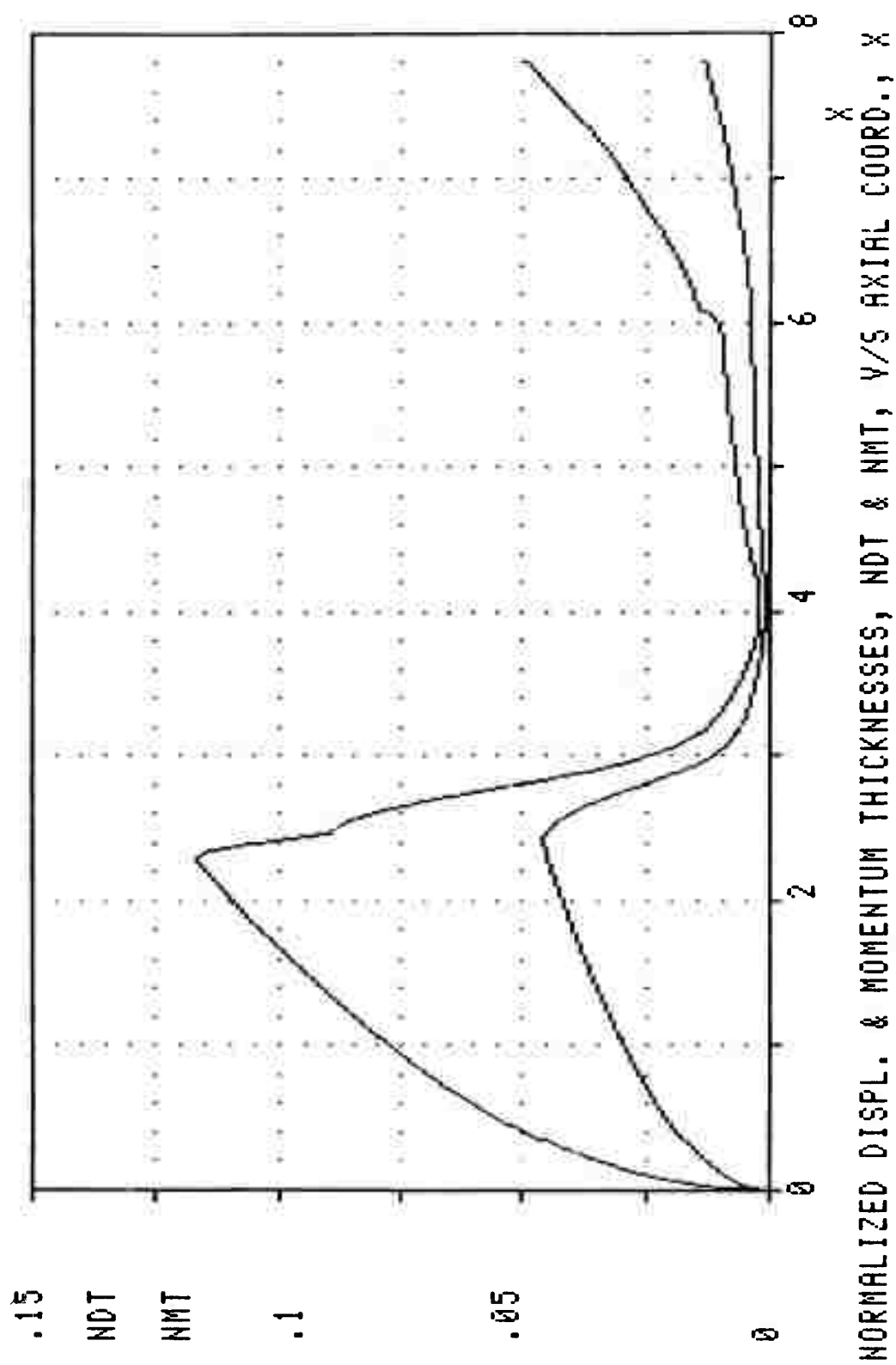


Figure 19. Normalized displacement thickness, NDT (upper curve), and momentum thickness, NMT (lower curve), v/s normalized axial coordinate, X, in the laminar C.S.M. venturi of Fig. 18. The Reynolds number at the inlet, based on the volume average velocity and duct radius, is: $Re_i = 700$. Boundary layer calculations are based on a quasi one-dimensional model of the flow in the duct.

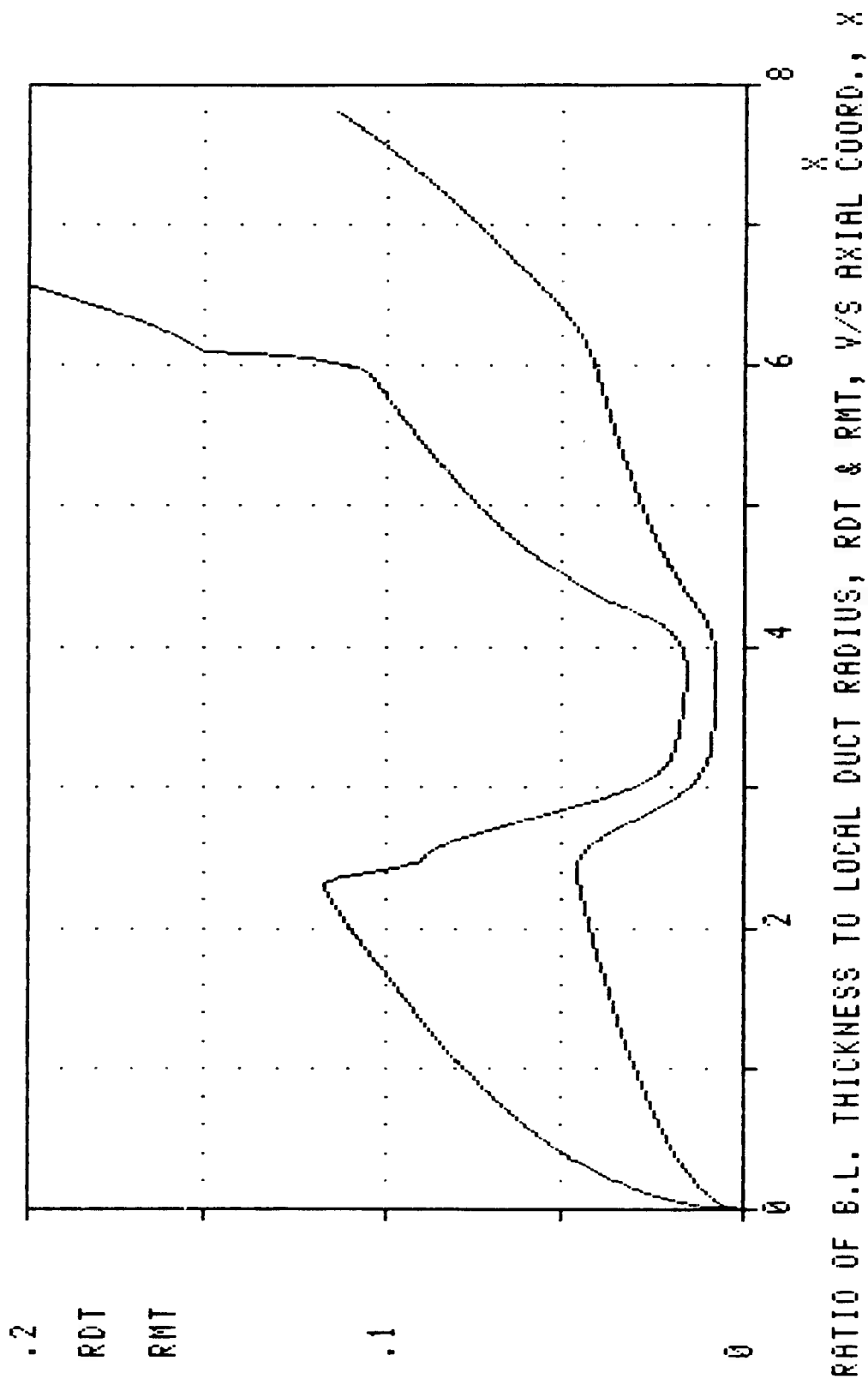


Figure 20. Relative displacement thickness, RDT (upper curve), and momentum thickness, RMT (lower curve), v/s normalized axial coordinate, X , in the laminar C.S.M venturi of Fig. 18. The Reynolds number at the inlet, based on the volume average velocity and the duct radius is: $Re_i = 700$ and the boundary layer thicknesses are expressed as fractions of the local duct radius. Boundary layer computations are based on a quasi one-dimensional model of the flow in the duct.

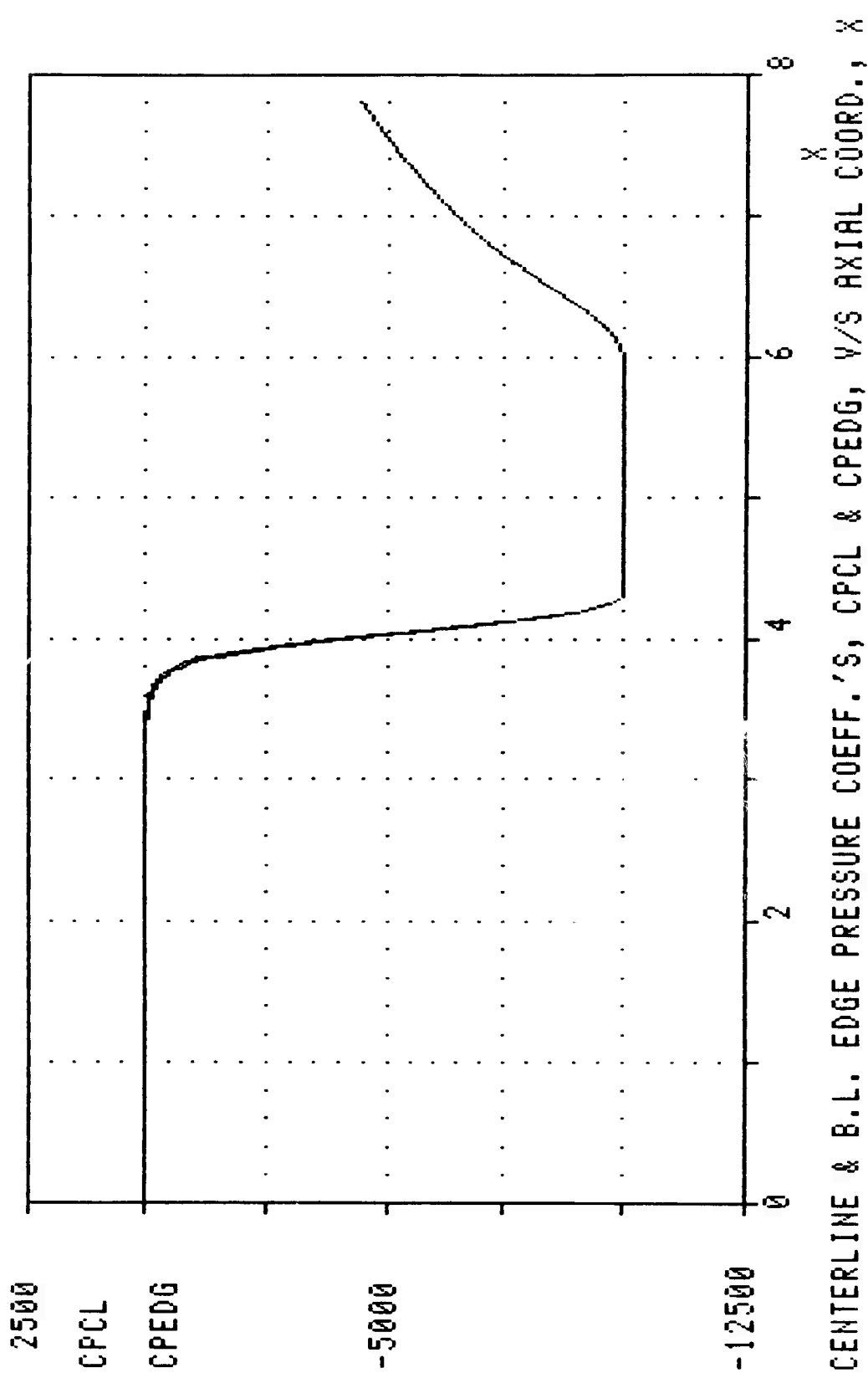
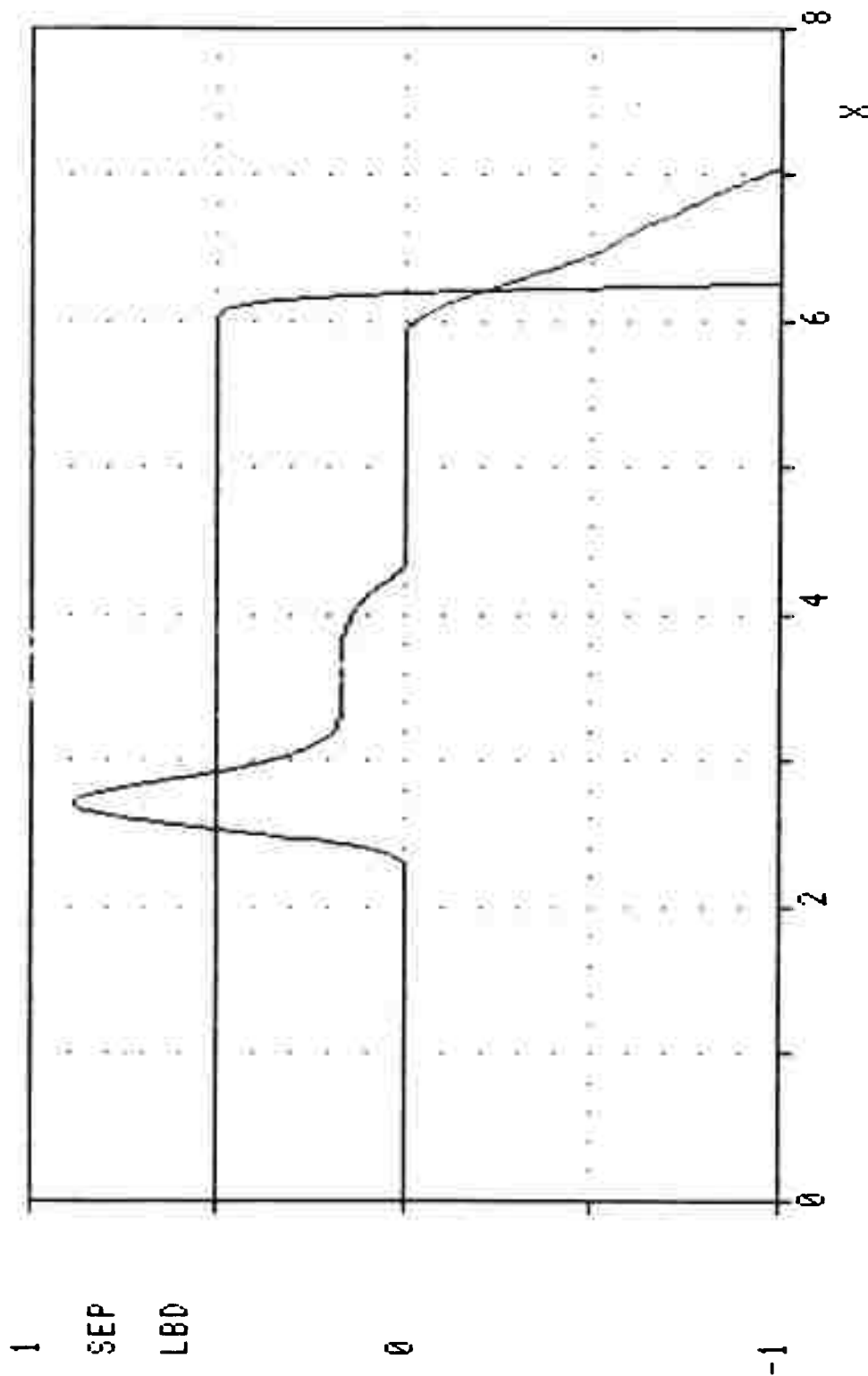


Figure 21. Centerline pressure coefficient, C_{pcl} [CPCL] (lower curve, essentially collapsed on the upper one), and boundary layer edge pressure coefficient C_{ped} [CPEDG] (upper curve), v/s normalized axial coordinate, X , for the C.S.M. Venturi of Fig. 18. Here the pressure is normalized w.r.t. the conditions at the duct inlet and computations are based on a quasi one-dimensional model of the flow.



SEPARATION & CORRELATION PARAMETERS, SEP & LBD, V/S AXIAL COORD., X

Figure 22. Stratford's laminar separation parameter, S [SEP] (upper curve), and Thwaites' shear and shape correlation parameter λ [LBD] (lower curve), v/s normalized axial coordinate, X , for the C.S.M. venturi of Fig. 18. Here Stratford's laminar separation equation is rearranged so that separation is predicted when SEP goes through zero or $\lambda = -.09$. Boundary layer computations are based on a quasi one-dimensional model of the flow in the duct.